Sound Speed Profiles from Vertical Array Data

David H. Berman
Department of Physics and Astronomy
University of Iowa
Iowa City, Iowa 52242
Steven N. Wolf
Code 7120
U. S. Naval Research Lab
Washington, DC 20375

March 22, 1994

N00014-93-1-2004

Abstract

A scheme for extracting sound speed information from vertical arrays in shallow water is examined. The scheme hinges on the covariance matrix of the pressures received at the array being diagonal in the modes of the water column, and involves computing second derivatives of the covariance. Conditions under which the covariance might be mode-diagonal are examined. It is found that without attenuation, it is unlikely to find mode-diagonal covariances. However with reasonable attenuations, the covariance will be dominated by the lowest mode. The scheme described here is applied to vertical array data taken in 1985.

I Introduction

The aim of this work is to examine the following question. Suppose that a vertical array of hydrophones is deployed in shallow water. A ship passes, or there is some other source of incoherent sound. What can be learned about the sound speed in the water as a function depth? If the sound speed profile can be determined, the normal modes of the ocean waveguide can be found and and then used to filter sound from unknown coherent targets in order to localize these in range and depth [1]. Furthermore, if the sound speed could be determined by listening to what is essentially noise, there would be no need to monitor the sound speed at the array continually with possibly expensive drops of XBT's etc.

The theoretical impetus for this work is the observation that if sound arriving at a vertical array is incoherent, so that modal amplitudes are uncorrelated with one another, then, if the array spans the water column and there is little penetration into the bottom, the eigenvectors of the covariance matrix of the pressures received at the hydrophones will be the normal modes of the ocean waveguide. As mentioned above the modes are useful for localizing sources, and for filtering signals in order to determine the time signature of the source. The point of the present investigation is to see what information can be gleaned from vertical arrays that do not span the water column and/ or are deployed where there is significant acoustic penetration of the bottom.

Sections II through V were written in 1993. Since then I have discovered that there was an error in my formula for transforming measured temperatures into sound speeds. In effect, sound speed from earlier work were low by about 100 m/s. Since then I have corrected this error and also used more reliable temperature data, but the qualitative results are unchanged. Section VI has been added. In that section a new and more successful method for smoothing data is described. In Section II a scheme will be described for extracting the sound speed from a mode-diagonal covariance matrix. In Section III situations which might produce a mode-diagonal covariance matrix will be discussed. In Section IV the scheme will be applied to simulated data and in Section V the scheme will be applied to data collected in 1985 off the coast of California near San Diego. The principle disadvantage of the method to be described below arises from the need to compute spatial second derivatives from array data. In particular, hydrophones on the array need to be well calibrated and well localized. Furthermore it appears that processes which might produce

sufficiently mode-diagonal covariance matrices are unlikely to be realized. However, mode stripping via attenuation may allow the scheme described here to work.

II Extracting the sound speed

In shallow water the sound pressure field $p(z)$ arriving at a vertical array can be represented as a superposition (linear combination) of normal modes $\{\phi_n(z), n = 1....N\}$,

$$p(z) = \sum_{n=1}^{N} a_n \phi_n(z). \tag{1}$$

In Section III conditions under which the modal amplitudes a_n might be uncorrelated will be discussed. For now simply assume that there is some averaging proceedure for which

$$\langle a_n a_m^* \rangle = A_n \delta_{n,m}. \tag{2}$$

If this is the case the pressure will be said to be mode-diagonal, and the covariance matrix Γ of the pressure received at hydrophones located at depths $\{z_i, i = 1...N_{ph}\}$ will be given by

$$\Gamma(z_i, z_j) \equiv \langle p(z_i) p^*(z_j) \rangle = \sum_{n=1}^{N} A_n \phi_n(z_i) \phi_n(z_j). \tag{3}$$

If the hydrophones are uniformly and closely spaced (with separation Δ) then discrete sums approximate integrals. Furthermore, if the hydrophones span the water column and the normal modes ϕ_n vanish or nearly vanish in the bottom, then the orthonormality of the modes gives

$$\sum_{i=1}^{N_{ph}} \phi_n(z_i) \phi_m(z_i) \Delta \approx \int_0^\infty \phi_n(z) \phi_m(z) dz = \delta_{n,m}. \tag{4}$$

This in turn means that

$$\sum_{j=1}^{N_{ph}} \Gamma(z_i, z_j) \phi_m(z_j) \Delta \approx A_m \phi_m(z_i). \tag{5}$$

In other words, the N_{ph} dimensional vector $\phi_m(z_i)$ is an eigenvector of the covariance matrix Γ with eigenvalue A_m/Δ. Hence to extract the acoustic normal modes from the incoherent covariance matrix Γ , simply find its eigenvectors. These eigenvectors can be

used subsequently to filter more coherent signals from unknown sources. For example, suppose the pressure at time t and depth z is given by

$$p(z,t) = \int \hat{f}(\omega)\exp(i\omega t)\sum_{n=1}^{N}\exp[-ik_n(\omega)r]\phi_n(z)\phi_n(z_s)/\sqrt{k_n r}\,d\omega \qquad (6)$$

Assuming that the source is reasonably narrow in frequency and centered on ω_o, write

$$\omega) \cdot \cdot \cdot n(\omega_o) + (\omega - \omega_o)/v_n, \qquad (7)$$

where v_n is the group velocity of the nth mode. Integration over frequency then gives a sum of delayed replicas of the source (delayed by r/v_n) and filtering with one of the modes gives a single replica of the source function:

$$\int \phi_m(z)p(z,t)dz \approx \phi_m(z_s)f(t - r/v_m)/\sqrt{k_n r}. \qquad (8)$$

The method of finding modes from the eigenvectors of Γ fails if the array does not extend over the entire region where the modes are appreciable. In this case one can make use of more known information about the modes, namely that they satisfy the separated wave equation,

$$\frac{d^2\phi_n}{dz^2} = -\left[\frac{\omega^2}{c(z)^2} - k_n^2\right]\phi_n. \qquad (9)$$

Forgetting for the moment that the hydrophone array is not continuous, differentiate the covariance matrix

$$\Gamma(z,z') = \langle p(z)p^*(z')\rangle = \sum_n A_n\phi_n(z)\phi_n^*(z'), \qquad (10)$$

twice with respect to z and subtract the result of differentiating twice with respect to z' to show

$$\frac{\omega^2}{c(z)^2} - \frac{\omega^2}{c(z')^2} = \left[Re\left(\frac{d^2\Gamma(z,z')}{dz'^2} - \frac{d^2\Gamma(z,z')}{dz^2}\right)\right]/Re[\Gamma(z,z')]. \qquad (11)$$

No terms involving the real parts of the horizontal wave numbers k_n appear because the covariance is diagonal in mode number. (In what follows attenuation is assumed sufficiently small that the modes are real to a good approximation and that the imaginary parts of the wave numbers k_n may be determined perturbatively.) Terms involving imagainary parts of the wavenumbers also involve the imaginary parts of the mode functions ϕ_n. Hence these terms are at least quadratic in the attenuations and are assumed negligible. A problem with this neglect might occur when sound speeds (assumed real in the water

column) at the depths z and z' are equal. Equation 11 is the main new result of this work. It implies that the sound speed profile can be determined to within an overall constant whenever second derivatives of the covariance matrix can be computed. It makes some sense that the result is ambiguous as to this constant, since adding a constant to the index of refraction does not change the propagation in the medium. Note that the sound speed is only determined at the array, and all that is assumed is that the covariance of the pressure field is mode-diagonal at the array. This is a considerably weaker assumption than the assumption of adiabatic propagation between source and receiver. However, hydrophones need to be sufficiently close to one another so that it is possible to determine reasonable approximations for the second derivatives, but not so close that measurement errors are larger than the small differences between the pressures at adjacent phones. In fact, computing the second derivatives is the primary disadvantage of the scheme implicit in Eq.11. Before turning to the difficulties in applying Eq.11, however, circumstances in which the covariance matrix might be mode-diagonal will be examined in the next section.

III When is the Covariance Mode-Diagonal?

Suppose that the ocean is not considered to be random, but that the source location is either unknown, or distributed uniformly in a horizontal plane, or is moving about and one averages the covariance over a time in whch the source has moved over a considerable range (neglecting Doppler effects). Assume that the ocean does not vary in azimuth and that the pressure is observed at a single frequency. The pressure at a depth z is given by

$$p(z) = \sum_n \exp(-ik_n r)\phi_n(z_s)\phi_n(z)\hat{f}(\omega)/\sqrt{k_n r}. \tag{12}$$

Form $p(z)p^*(z')$ and average over ranges using

$$\frac{1}{\rho}\int_{R-\rho/2}^{R+\rho/2} ...rdr$$

to get

$$\Gamma(z,z') = \sum_{n,m} \exp[-i(k_n - k_m^*)R]\frac{\sin[(k_n - k_m^*)\rho/2]}{(k_n - k_m^*)\rho/2}|\hat{f}(\omega)|^2\phi_n(z_s)\phi_m(z_s)\phi_n(z)\phi_m(z')/(R\sqrt{k_n k_m^*}) \tag{13}$$

Note that the horizontal wave numbers might have imaginary parts as a result of attenuation, intrinsic or otherwise. In the double sum, as $\rho \to \infty$ the sinc function becomes a Kronecker delta in mode number if the wave numbers are real. If the wavenumbers are complex, denote their imaginary parts by $-\alpha_n$. It can be seen that if

$$|(Re(k_n) - Re(k_m))\rho| \gg \pi$$

and

$$(\alpha_m + \alpha_n)\rho \ll 1$$

then the terms in the double sum for which $n \neq m$ will be much smaller than the terms $n = m$. This is to say that the covariance matrix will be diagonal in mode number if there is little attenuation over the averaging distance ρ and if the modes have a chance to "beat" against one another in the averaging distance.

Instead of averaging over range, it is also possible to average over frequencies to produce a covariance matrix which is nearly diagonal in mode number. If $\hat{f}(\omega)$ is a stationary random process then

$$\langle \hat{f}(\omega)\hat{f}^*(\omega')\rangle = S(\omega)\delta(\omega - \omega'). \tag{14}$$

Assume that the spectrum of the source, $S(\omega)$ is flat about $\omega = \omega_o$ over the bandwidth $\Delta\omega$ and vanishes for $|\omega - \omega_o| > \Delta\omega/2$. Use Eq.7 to expand the phase of the pressures Eq.12 about the center frequency of the source, ω_o, but assume that the frequency dependence of the modes and the of the denominators in Eq.12 can be ignored. Using these assumptions, and forming

$$\Gamma(z, z') = \int d\omega \int d\omega' \langle p(z, \omega) p^*(z', \omega') \rangle$$

gives

$$\Gamma(z, z') = \sum_{n,m} \exp[-i(k_n - k_m^*)R] \frac{\sin[(1/v_n - 1/v_m^*)R\Delta\omega/2]}{(1/v_n - 1/v_m^*)R\Delta\omega/2}$$

$$S(\omega_o)\phi_n(z_s)\phi_m(z_s)\phi_n(z)\phi_m(z')/(R\sqrt{k_n k_m^*}). \tag{15}$$

This form of Γ is the same as that given by range averaging in Eq.13 except that here the argument of the sinc function is now $(1/v_n - 1/v_m^*)R\Delta\omega/2$. If $\Delta t = 1/\Delta\omega$, the duration of a pulse, and if the group velocities are real, then the condition giving rise to a kronecker delta in mode number is

$$|(Re(r/v_n) - Re(r/v_m)\Delta\omega)| = |(t_n - t_m)/\Delta t| \gg \pi.$$

In other words the covariance will be diagonal in mode number if the times of arrival of pulses in modes n and m are separated by a time much greater than that of the original pulse width. It would seem that one could choose the range of transmission R sufficiently large so that this is the case.

Finally there is a third, almost trivial, case in which the covariance will be diagonal in mode number. If the distance between source and receiver is sufficiently large and if there is high attenuation arising either from frictional losses in the bottom or from loss of coherence at the various interfaces in the ocean, then only the first mode will be appreciable at the receiver. If so, the covariance matrix will be of the form

$$\Gamma(z, z') = A_o\phi_o(z)\phi_o(z'). \tag{16}$$

and Γ is trivially diagonal in mode number. This case is mentioned here because it appears that the data set available for testing the scheme outlined above is in fact dominated by the first mode. Furthermore, the simulations discussed below indicate that averaging over range might require unrealizable averaging distances if there is no attenuation.

IV Simulated Covariances

In this section simulated covariances are examined in order to determine the feasibility of applying Eq.(11) to determine sound speed profiles. In all cases normal modes are computed using the normal mode code KRAKEN [2, 3]. Since computation of fields at different ranges is considerably easier than computation of fields at different frequencies, only range averaged covariance matrices will be considered here. Using simulations it is relatively easy to see how limited averaging affects Eq. 13 and the sound speed inferred from such a covariance matrix.

In all cases to follow we will deal with a sound speed profile similar to the sound speed in the part of the ocean from which the data in the next section was taken. Specifically we assume shallow water 18 m deep with a source centered on 400 Hz. The sound speed in the water column varies from 1415 m/sec at the top to 1404 m/sec near the bottom. Details are given in Table I. In the actual experiment, source and receiver were separated by 3.7 km. The bottom properties were not measured; however, it is known that the bottom consisted of coarse sand. One of the main points of the present discussion is that the attenuation in the bottom and the roughness of the sea surface and bottom interfaces are critical for deciding if the covariance is mode diagonal. Hence simulations for various attenuations and roughnesses will be considered.

We first examine the question of how much averaging needs to be done in order that the covariance be diagonal in mode number. Suppose that there is no attenuation and that somehow the sound could be measured at all depths, including in the ocean bottom. Then the covariance matrix would be diagonal in mode number if the matrix

$$A_{n,m} = \exp[-i(k_n - k_m^*)R]\frac{\sin[(k_n - k_m^*)\rho/2]}{(k_n - k_m^*)(\rho/2)\sqrt{k_n k_m}} \tag{17}$$

is diagonal. One can see how much mixing of modes there is by looking at the eigenvectors of A. To apply Eq.11 these eigenvectors should be of the form

$$e_j^{(n)} = \delta_{n,j}.$$

Figure 1 shows a plot of Re(A) when $R = 3700m$, and $\rho = 1000m$ using the wave numbers in table II. The matrix A appears to be reasonably diagonal. However, Fig 2 shows that the first four of seven eigenvectors of A significantly mix adjacent modes. In this case it

is unlikely that either the second-derivative scheme for determining the sound speed will succeed, or that the eigenvectors of Γ will correspond to the modes of the water column. Fig 3 displays the eigenvectors of the matrix A when ρ = 10,000 m. The first and fourth eigenvectors are dominated by a single mode; the second and third eigenvectors show significant mixing of modes. When ρ = 100 km, all of the eigenvectors of A have adjacent modes mixed in with amplitudes less than 1 percent. One could say that the case of ρ = 10000 m is marginal, and that to extract the modes or the sound speed profile one should have the averaging distance ρ greater than 10,000 m for the wavenumber separations of this problem.

Similar computations could be made for the case of frequency averaging. However, we can see that A is almost sufficiently diagonal when the argument of the sinc function is about

$$(k_1 - k_2)\rho/2 \approx .02 * (10000)/2 = 100.$$

In the case of frequency averaging it would seem that one needs (See Eq.15)

$$|(R/v_1) - (R/v_2)| * \Delta\omega/2 \approx 100.$$

Using $R = 3700$ and $v_1 = 1410$, $v_2 = 1395$ means that the bandwidth should satisfy

$$\Delta f > 1000 Hz.$$

Unfortunately the bandwidth in the experiment from which data in the next section is derived was only 80 Hz.

Consider now how the sound speed can be extracted. Using an averaging distance $\rho = 100km$ we would think that the covariance matrix would be sufficiently mode diagonal. In accordance with the experimental data to be described in the next section, consider an array of 25 equally spaced hydrophones located at depths of .11 m to 16.502 m and spaced .683 m apart. Compute second derivatives using fifth-order finite differences and apply Eq. 11. The inferred indices of refraction are adjusted so that mean of the input profile is nearly the same as that of the inferred profile. The result of this proceedure is shown in Fig. 4. The point here is that without noise, and when the covariance matrix is nearly mode-diagonal, the scheme implied by Eq. 11 only gives a marginal fit. However, if the covariance is constructed from only the first mode, the fit to the input sound speed

is much better. (See Fig 5.) The discrepancy here between the inferred sound speed and the sound speed used to construct the simulations must be attributable to the process of forming second derivatives from fifth-order finite differences. For comparison with cases involving attenuation, Fig. 6 shows the covariance matrix itself for this single mode.

Now suppose that there is even less range averaging to make the covariance mode-diagonal. The proceedure just described, but now with $\rho = 10km$ yields the results shown in Fig. 7. The inferred sound speed profile is not too different than that obtained with $\rho = 100$ km. It is possible that in these cases the higher-order modes are not sampled well enough to allow good approximations of the second derivatives. For this case, the 25×25 covariance matrix is plotted as a surface in Fig. 8. However, in Fig. 9 is plotted the covariance matrix computed with $\rho = 1km$, but now with more realistic roughness and attenuations. This covariance has a considerably different shape than than the covariances computed without attenuation. In fact, it is dominated by the lowest, least attenuated mode. This can be seen in Table 3 which shows the eigenvalues of this matrix, and by comparing Fig. 6, the covariance computed with the first mode. Thus this matrix is almost trivially mode-diagonal, since there is virtually only one mode, and the results of applying our extraction scheme should be better than those obtained in Fig. 4. This is demonstrated in Fig. 10. Note that when the covariance is dominated by a single mode, the real part will be positive. Significant contributions from other modes will cause the real part to change sign for some matrix elements. Finally, the simulations shown in Figs. 9 and 11 demonstrate that the shape of the covariance matrix when there is bulk attenuation and the shape of the covariance matrix when there is both bulk attenuation and surface roughness are noticeably different. The latter seems to be even more dominated by a single mode.

V Data

An experiment which took place off the coast of California near San Diego provided a simple data set taken with a vertical array. Unfortunately the parameters of this experiment were marginal at best for the purpose of the extraction scheme described here. In the experiment a source located on the bottom in 18 m of water emitted a pseudo-random signal of nominal bandwith 80 Hz. The signal was received on a vertical array located

3.7 km from the source. Divers indicated that the bottom was nearly featureless, but there were no detailed measurements of the bottom roughness nor of the attenuations and sound speeds in the bottom. What is known is that the bottom consisted of coarse sand. Temperature profiles were measured near the receiving array near the time of the experiment. However, these were recorded in plots of isotherms in depth and time. The sound speed which is compared with the results of our extraction scheme was derived from these rather crude plots. It is this sound speed profile which was used in the simulations of the previous section. However, the most severe limitation on the experimental data is that the hydrophones were not well calibrated and, in fact, of the 25 phones on the array about 5 were nearly dead. Fig. 12 shows a plot of the real part of the covariance matrix filtered in an 80 Hz band centered on 400 Hz. The deep creases in Fig. 12 show that about five of the hydrophones were not functioning properly. To try to overcome this problem, the results of the 'bad' hydrophones were scaled so that the intensities of the scaled output interpolated the intensities of neighboring hydrophones located on each side. (This, of course, does not really solve the problem, since it is second derivatives we are after.) Fig. 13 shows the result of this interpolation scheme. This 'corrected' matrix was used to extract the sound speed profile. Note that this matrix is much more similar to the matrices of Figs. 6 and 9 than to those of Figs. 8 and 11. It seems to be dominated by a single mode. One can surmise that attenuation is playing a dominant role here and that the averaging over the frequency band of 80 Hz is not critical.

The imaginary part of this covariance matrix did not vanish. This could indicate either that the array was not vertical or that in fact the covariance is not diagonal in mode number. If the array were not vertical the extraction scheme can to some extent correct for this by multiplying by a phase phase factor designed to minimize the imaginary parts of the resulting covariance elements. There is not much to be done if the covariance is not mode diagonal.

At this frequency, the hydrophone spacing of .68 m represents about 1/5 acoustic wavelengths. Thus one might think that the sound field is well sampled by the array. However, the simulations indicate that this might not be the case. For the fith mode, for example, nodes will be spaced about 4.5 m apart. There are 4.5/.683= 6.6 sample points between nodes. As indicated above, the contributions from higher modes do not yield good sound speed estimates at this sampling rate.

Despite these difficulties we tried to apply the extraction scheme. Various smoothing methods were tried to clean up the data, but the most successful seemed to be using a 5 point finite difference formula to compute second derivatives and then applying a Gaussian filter to further smooth the arrays of estimated second derivatives [4]. The results are shown in Fig. 14 The estimations near the endpoints of the array were wildly wrong in the case of simulations and in this application to data. Extracted values near the ends are therefore not plotted. Except for the values of the sound speed near the ends of the array, the sound speed extracted in Fig. 14 pretty much follows the trends of the measured sound speed. However, different smoothing schemes and different ways of estimating derivatives gave quite different results. Given the poor quality of the data here, it might not be surprising that a reasonable sound speed is hard to extract.

VI An Alternative Numerical Scheme

The finite difference scheme just described only depends on assumptions about the field over the array. However, in practice, the variation of the second derivatives across the array is so variable that some smoothing is required even to produce the somewhat disappointing results presented here. It is particularly difficult to obtain anything resembling reasonable results for the sound speed profile near the ends of the arrays. In the computations presented here, the following second derivatives were computed:

$$d^2\Gamma(z_i, z_{i+1})/dz_i^2 \tag{18}$$

and

$$d^2\Gamma(z_i, z_{i+1})/dz_{i+1}^2 \tag{19}$$

for all indices i in the array. The sequence of these second derivatives was then smoothed using a Fourier technique described in Numerical Recipes (SMOOFT) [4]. This smoothing implicitly makes assumptions about the behavior of the covariance matrix beyond the array. By changing the degree of smoothing, and changing the list of hydrophones used in the array, a wide variety of inferred sound speed profiles could be obtained, all with unrealistic values near the ends and often completely unrealistic even in the middle of the array. For this reason another scheme for smoothing the covariance was investigated which will now be described.??

Originally it was thought that if the array spans the water column and if there is little penetration into the bottom, then the eigenvectors of the covariance matrix (if it is mode diagonal) will be the acoustic modes supported by the sound speed profile. This is so because if there is little penetration into the bottom, the modes will be orthogonal over the array aperture. For an array which does not span the water column or for modes that penetrate the bottom, the modes will not be orthogonal over the array aperture. Nevertheless, one can still look at the eigenvectors of the covariance matrix and smooth these by fitting them with modes of a hypothetical sound speed profile. It is then an easy matter to compute the second derivatives of the fitted eigenvectors either by using the separated wave equation or by further fitting with say, the modes of a Pekeris model whose second derivatives can be found analytically.

Returning to Fig. 12, instead of interpolating between 'bad' hydrophones, now simply

drop them from consideration. In using a finite difference scheme to find derivatives, it was almost essential that the points of the array be uniformly spaced. If the eigenvectors are going to be fitted with smooth functions, the points of the array need not be uniformly spaced. In Fig. 15 some cross sections of the covariance plotted in Fig. 12 are presented. It is clear that phones {2,7,11,16,20,23,24} are at best weak and these will be dropped from consideration. The eigenvalues and first few eigenvectors of the real part of the resulting decimated covariance matrix are presented in Fig. 16. First note that the first four eigenvalues are considerably larger than the remaining eigenvalues. This probably indicates that the field at the array is dominated by linear combinations of the propagating acoustic modes and that there are likely only four of these. Moreover, it is clear that the eigenvectors resemble the normal modes of the separated wave equation, showing 0, 1, 2 and 3 zero crossings. Although these eigenvectors must be orthogonal to one another, the modes of the acoustic environment which produced the covariance matrix will not be orthogonal over this array aperture. Because we are dealing with a source-free acoustic field at the array, we can be sure that the field must have continuous derivatives along the array. Hence some degree of smoothing is called for. In addition, second derivatives must be bounded roughly by the size of the field times the largest vertical wavenumber squared. For these reasons reconstruct the covariance matrix using smoothed versions of the first 3 or 4 eigenvectors.

Smoothing the eigenvectors need not be entirely arbitrary. The eigenvectors must be some combinations of modes of the actual sound speed profile and bottom parameters. A guess can be made as to the profile–say it is a constant to begin with–and the bottom parameters. We guess the bottom density to be 1.5 g/cc and the bottom sound speed to be around 1700 m/s. The first few modes of this profile can be used to fit the first few eigenvectors of the covariance. By using only the first few modes of the profile we are assured that we are not trying to fit with functions which have large second derivatives. (If we were to fit with polynomials we would want to make a least square fit but with a constraint to the effect that the second derivative of the resulting fit be bounded.) In fact the modes used to fit the eigenvectors in the first approximation are modes of a Pekeris problem. For sound speed profiles with more structure, the modes can be computed using the KRAKEN normal mode program. It is then convenient to fit the KRAKEN modes (given at discrete points) with analytic Pekeris modes associated with a large water

column. In this way the 4 or so propagating modes can be fit with 6 or 7 Pekeris modes. The later are simply sinusiods (although not orthogonal over the array aperture) whose second derivatives are easily computed.

Thus if the eigenvectors of the covariance matrix Γ are $e^{(n)}$ with corresponding eigenvalues λ_n, then approximate the vectors $e^{(n)}$ by

$$e_i^{(n)} \approx \sum_{m=1}^{M} a_m^{(n)} \phi_m(z_i). \tag{20}$$

In this equation, the $\{\phi_m\}$ are the normal modes of a hypothesized acoustic problem, and the coefficients $\{a_m^{(n)}\}$ are determined by a least square fit. Continuous functions $g^{(n)}(z)$ are determined by

$$g^{(n)}(z) = \sum_{m=1}^{M} a_m^{(n)} \phi_m(z). \tag{21}$$

The covariance matrix is then continuously approximated by

$$\Gamma(z, z') \approx \sum_{n=1}^{N} \lambda_n g^{(n)}(z) g^{(n)}(z'). \tag{22}$$

The number of modes M used to approximate the eigenvectors $e^{(n)}$ need not be the same as the number of vectors N used to reconstruct Γ. The modes ϕ_m are determined at discrete points by a normal mode code and then themselves fitted with modes of a Pekeris problem. In order to have a good fit of the modes, the water depth of this Pekeris profile is taken to be larger than the water depth in the experiment or in the profile used to produce the modes ϕ_n. Taking the water depth (the depth of the upper layer) in the Pekeris model to be about 1.5 or 2.0 times the actual water depth seemed to be adequate. Thus while there might be only 4 propagating modes in the experiment, 6 or 7 Pekeris modes might be used to fit these modes.

The first few eigenvectors of the covariance matrix without "bad" phones and their continuous approximations using only 3 modes of the environment indicated in the caption are shown in Fig. (17). Fig. (18) shows the reconstructed covariance matrix of Eq.22 which is to be compared to the original covariance in Fig.(12). Using Eq. (11) to determine a sound speed profile with this approximate but smoothed covariance gives the results shown in Fig. (19) where it is compared with the nominal sound speed profile determined from temperature data. The fit shows the general trend of the measured sound speed, but

because only a 3 modes are used to reconstruct the covariance, it can hardly be expected to reproduce details of the profile. One might think to use more modes to fit the eigenvectors of the covariance. Fig.(20) shows that indeed using 4 modes to fit the eigenvectors gives a close approximation of the eigenvectors. However, since the eigenvectors are necessarily "noisy," the second derivatives of this closer fit need not be closely related to the second derivatives of the acoustic field. This is demonstrated in Fig. (21) which shows the sound speed profile derived from a 4-mode fit to the eigenvectors. In this context a closer fit is not a better fit.

One attraction of the scheme just described is that having derived an approximate sound speed profile, one can then use this profile to generate new modes with which to fit the eigenvectors of the covariance matrix. The new modes can then be used to produce a second approximation to the profile. Unfortunately there is no guarantee that this iteration procedure converges, or even if it converges, that it converges to the correct sound speed profile. In fact it is my experience that iterating does not necessarily improve the inferred profile. Figure (22) shows the second iteration of this procedure using three KRAKEN modes. The trend of higher iterations is away from the nominal profile.

There are other variables to adjust in this method to try to infer a sound speed profile. The bottom model that is used was only a rough guess as to the actual bottom. Suppose instead we fit with modes which come from a model having bottom sound speeds in two layers of 1650 m/s and 1750 m/s and a density of 1.6 in the first and 1.7 in the second which begins at 28 m. The resulting inferred profile in the water column is shown in Fig.(23) It appears that by reducing the bottom sound speed so that there is more penetration into the bottom results in a better estimate of the sound speed in the water. Continuing in this direction, suppose the bottom begins with a sound speed of 1600 m/s and increases to 1700 m/s at a depth of 28 m. In this layer suppose the density is 1.25. Below 28 m suppose the density is 1.75 and the sound speed is constant at 1700 m/s. The inferred profile using modes derived from this bottom model and a constant sound speed of 1524 m/s is shown in Fig. (24). It appears that the choice of bottom model has more effect on the resulting inferred profile than does the limited variation possible in the assumed sound speeds in the water. This observation is consistent with Michael Collins' observations using simulated annealing to infer sound speed profiles: it is easier to infer bottom properties than details of the sound speed in the water. Thus, in the present case, if the measured profile in the

water is accepted, then it might be inferred that the bottom allows more penetration than a bottom consisting of a single half-space with sound speed of 1800 m/s and density of 1.5.

Note that in Figures 17 and 20 the parts of the eigenvectors corresponding to the deeper hydrophones, are rather poorly fit. For this reason, perhaps one might try omitting not only phone 24 but also 22 and 23. Using a Pekeris model with sound speed in the bottom of 1800 m/s and density in the bottom of 1.5 g/cc to produce modes with which to fit the eigenvectors gives the sound speed shown in Fig. 25. Athough this sound speed appears qualitatively different from that of Fig. 24, and although it seems remarkable that this sound speed seems to agree with the measured sound speed at the top, middle and bottom of the array, the maximum error is still about 2 m/s. This is about the same as indicated in Fig. 24. Here the bottom model is relatively less penetrable than that of Fig. 24. Furthermore, examination of the eigenvectors shows that by omitting phones 22,23,and 24, the eigenvectors shifted slightly, but the quality of the fits of the eigenvectors was not noticeably improved. See Fig. 26. Finally, in the previous attempts at reproducing the observed sound speed profile, having a more penetrable bottom seemed to provide better fits. Omitting phones 22,23,and 24 and using a bottom profile that increases linearly from 1650 m/s at 18 m to 1750 m/s and 28 m with a density of 1.5, and then increasing to a constant sound speed of 1800 m/s with a density of 1.75 below 28 m gives the result shown in Fig 27. One should probably stop here, but to illustrate that iterating does not necessarily give better results, Fig. 28 shows the seventh iteration of this profile (keeping the bottom fixed). There was very little difference between the sixth and seventh iterations ($< .1$ m/s).

In summary, with a good estimate of bottom properties it is possible to infer trends in the sound speed profile in the water using the covariance of the field received along a vertical array. With this information it is possible to find the modes of the acoustic field. However, a close fit of the sound speed profile is not possible. On the other hand, a close fit might not be necessary, since the modes are not so sensitive to the sound speed profile, and it is the modes that are used for spatial filtering. In fact even a constant sound speed profile gives qualitatively correct modes; even when the modes are not orthogonal over the aperture of the array, the eigenvectors of the covariance matrix look like modes. The utility of the the scheme described here might not be as a tool for finding the sound speed in the

water, but rather it might be more useful for making inferences about bottom properties. However, this can only be the case if all hydrophones are giving reliable measurements. Significantly better approximations of the sound speed resulted when certain phones were omitted. A priori, however, there seems to be little justification for omitting phones 22, and 23. Nevertheless, given the crudeness of the measurments as indicated by the noisiness of the covariance, it is remarkable that the sound speed profile can be inferred so precisely.

VII Acknowledgements

This work was supported by a grant from the Naval Research Laboratory, Washington, DC

References

[1] T. C. Yang, "A method of range and depth estimation by modal decomposition," J. Acoust. Soc. Am. **82**, 1736-45 (1987).

[2] Michael B. Porter, "The KRAKEN normal mode program," SACLANT Undersea Research Centre Memorandum (SM-245) / Naval Research Laboratory Mem. Rep. 6920 (1991).

[3] Michael B. Porter and Edward L. Reiss, "A Numerical Method for Ocean Acoustic Normal Modes," J. Acoust. Soc. Am. **76** 244-252 (1984).

[4] W. H. Press, B. Flannery, S. Teukolsky and W. Vettering, *Numerical Recipes* (Cambridge University Press, 1986) pp. 495-97.

[5] The sound speed profile used in this section differs from that in previous sections in that is it derived directly from temperature data. In the previous section, temperatures were taken from a faulty contour plot of temperatures and time. Furthermore there was an error in the code used to transfrom temperatuer to sound speed that resulted in sound speeds about 100 m/s too small. It does not seem worth while to repeat these plots using correct sound speeds since the qualitative results will be unchanged.

Table Captions

1. Sound speeds as a function of depth used to construct the simulations in this paper. This is a three layered medium. Bottom and sub-bottom are characterized by discontinuities in either density or sound speed, but these quantities are constant within these layers. In some of the simulated results attenuation was added to the bottom and sub-bottom and roughness to the interface.

2. The group and phase velocities of the propagating modes of the profile of Table 1 at 400 Hz.

3. The first six eigenvalues of the covariance matrix of Fig. 9. It is likely that the smallest values are numerical noise.

Figure Captions

1. The matrix A of Eq. 17 when $R = 3.7$ km and $\rho = 1$ km.

2. The first four eigenvectors of the matrix A displayed in Fig. 1. Note how there is mixing of the basis set.

3. The first four eigenvectors of A computed with $R = 3.7$ km and $\rho = 10$ km.

4. Comparison of the extracted sound speed profile, (open squares) with the sound speed (filled diamonds) used to construct the covariance matrix. In this case the covariance was contructed with the six propagating modes at a range of 3.7 km and using an averaging distance of 100 km. No attenuation or roughness was used. The phase velocities of these modes are listed in Table II.

5. The extracted sound speed as in Fig. 4. Now only the first mode was used to construct the covariance.

6. The real part of the covariance matrix ($\times 10^6$) used in Fig. 5. Cross-sections parallel to say the x-z plane show the shape of the lowest order normal mode.

7. The extracted sound speed as in Fig. 4. Here the averaging distance ρ was 10 km. The result is virtually the same as when the averaging distance was 100 km.

8. The real part of the covariance matrix ($\times 10^6$) used in Fig. 7. With all modes present and no attenuation, the covariance shows considerable structure across the diagonal and little structure parallel to the diagonal. Note that the covariance matrix can become negative.

9. The real part of the covariance matrix ($\times 10^6$) computed as in Fig. 8. However, here the averaging distance ρ was 1 km and the environment included both surface roughness and attenuation in the bottom. The bottom attenuation in both layers was taken to be .47 dB/(kHz-m). The rms roughness at the top interface was .25 m, at the water-sediment interface .5 m, and at the bottom interface .5 m. Note the similarity to the single-mode covariance of Fig. 6.

10. The sound speed inferred from the covariance of Fig. 9.

11. The real part of the covariance computed as in Fig. 8. Here the averaging distance was 3 km and there is no surface roughness. The attenutation in the bottom was .15 dB/(kHz-m).

12. The real part of the covariance ($\times 10^-11$) taken from experiment near San Diego. The deep creases indicate that a number of the hydrophones were not working properly.

13. The same data as in Fig. 12 with results of the dysfunctional hydrophones scaled by factors which gave smooth intensities.

14. The sound speed inferred from the covariance of Fig. 13. The extreme behavior at the ends of the array arises from the smoothing scheme and the difficulty of finding derivatives at the ends of arrays.

15. Three cross sections of the covariance matrix corresponding to C(i,5), C(i,11), C(i,19).

16. a) Eigenvalues of the decimated covariance matrix: hydrophones {2,7,11, 16,20,23,24 } removed. The remaining matrix is 18 by 18. b) The first three eigenvectors of the decimated covariance matrix plotted against the depth of the associated index.

17. a) Fit of the first eigenvector with Pekeris modes. Bottom sound speed is taken to be 1800 m/s. b) Fit of second eigenvector. c) Fit of third eigenvector.

18. Reconstructed covariance matrix using the first three smoothed eigenvectors and the corresponding eigenvalues.

19. Inferred sound speed from the smoothed covariance in Fig. 18, using equation 11.

20. Fits of the first three eigenvectors of the covaricance matrix using the first four instead of the first three modes of the Pekeris model described above.

21. The resulting sound speed profile using Equation 11 using 4 modes to fit eigenvectors.

22. The sound speed profile using modes of the profile shown in Fig. 19 to fit the first three eigenvectors of the covariance matrix. The glitch near the bottom is likely a result of ill conditioning in the fit of the modes with Pekeis modes. It is not present when the Pekeris modes come from a water depth of 1.5 times the true water depth rather than 1.75 time the true depth as shown here.

23. The sound speed profile that results when the first three eigenvectors are fit with three modes from a model with c=1524 m/s in the water to 18 m, with c = 1650 m/s and ρ = 1.6 g/cc between 18 m and 28 m and c = 1750 m/s , $\rho = 1.7 g/cc$ in a layer extending from 28 m to infinity.

24. The sound speed profile using a bottom that varies linearly (in n^2) from c=1600 m/s to c=1700 m/s at 28 m with density of 1.25 g/cc and below 28 m, c = 1700 m/s and density is 1.75 g/cc.

25. Fits of the eigenvectors omitting phones 22 and 23 in addition to the phones listed above using modes from a bottom model in which the sound speed varies linearly from 1650 m/s to 1750 m/s between 18 m and 28 m with density 1.5 g/cc and with sound speed of 1800 m/s and density 1.75 below 28 m.

26. The sound speed profile after seven iterations from the profile shown in Fig. 27.

Table I

Depth	Sound Speed	Density
.00	1415.00	1.03
.75	1414.83	1.03
3.00	1413.53	1.03
5.75	1412.20	1.03
7.00	1410.86	1.03
10.75	1409.52	1.03
11.25	1408.11	1.03
13.00	1406.70	1.03
16.50	1405.29	1.03
18.00	1404.25	1.03
Bottom:		
18.00	1700.00	1.50
28.00	1700.00	1.50
Sub-botton		
28.00	1700.00	2.10

Table II

MODE	GROUP VEL	PHASE VEL
1	.140406E+04	.177627E+01
2	.138978E+04	.175357E+01
3	.136344E+04	.171546E+01
4	.132485E+04	.166096E+01
5	.127481E+04	.158776E+01
6	.123629E+04	.149634E+01

Table III: First 6 Eigenvalues of Covariance

No.	Eigenvalue
1	9.2 E-5
2	5.9 E-6
3	6.9 E-9
4	-2.1 E-9
5	-1.9 E-9
6	-2.0 E-9

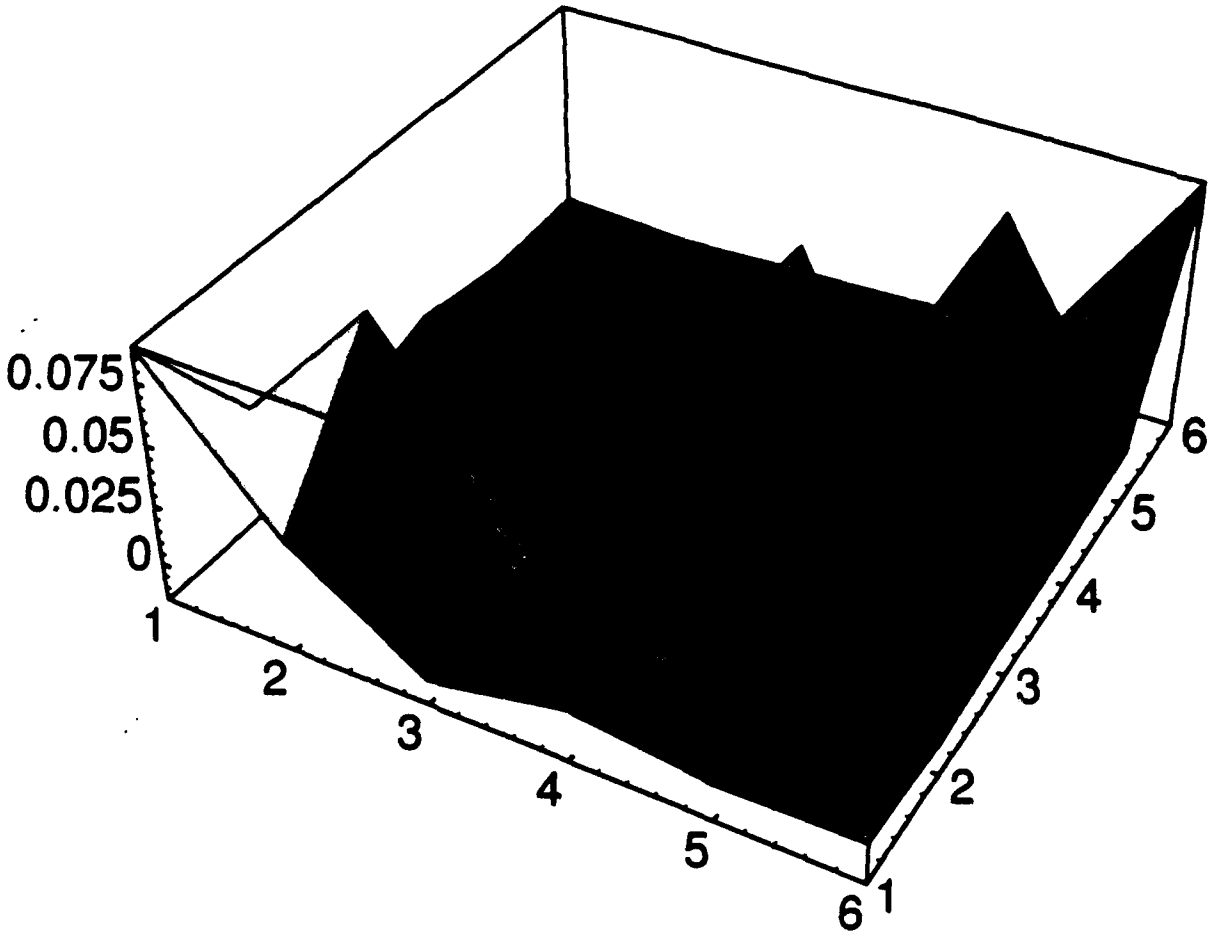

F 2 1

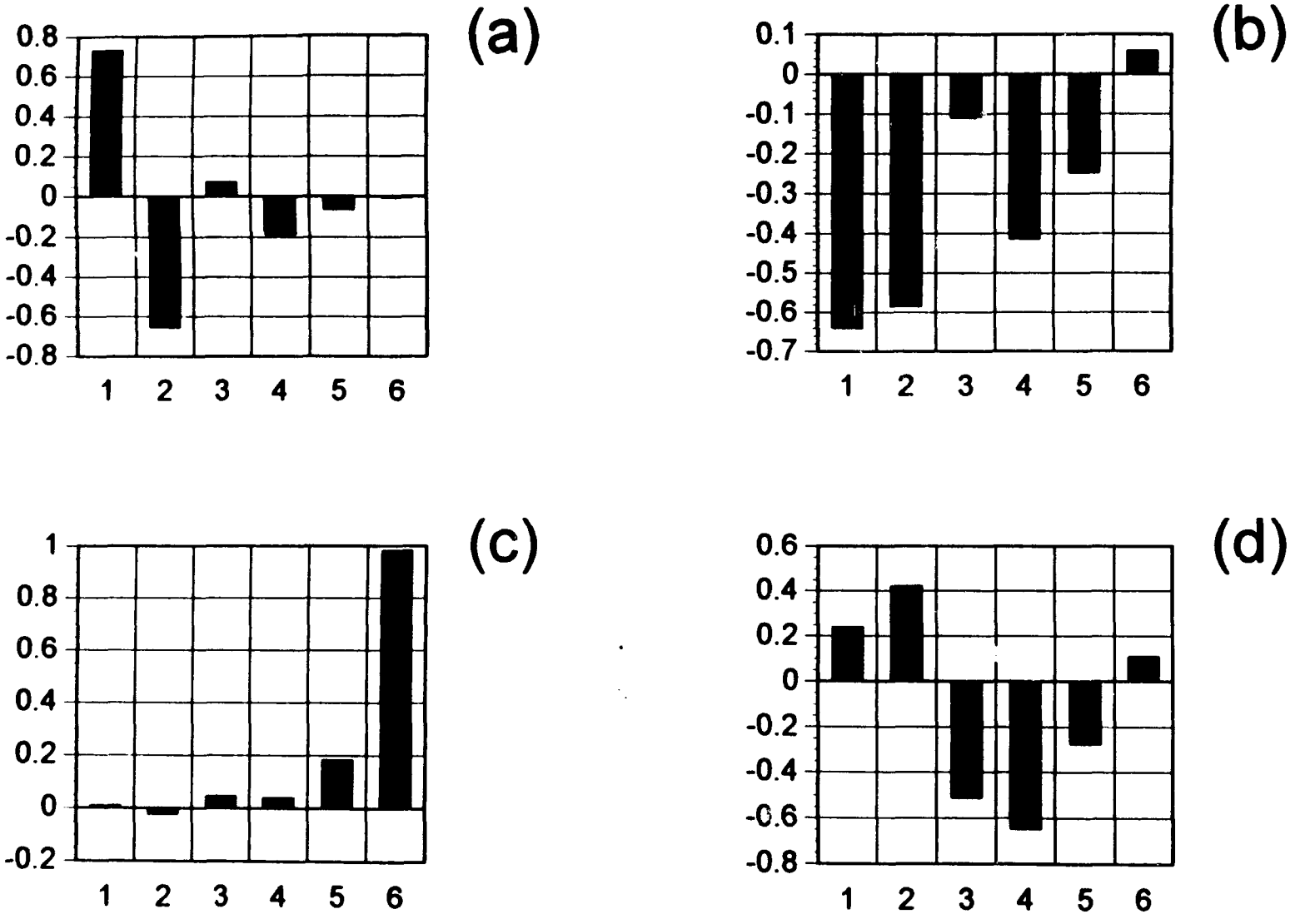
(a)
0.8
0.6
0.4
0.2
0
-0.2
-0.4
-0.6
-0.8
1 2 3 4 5 6
(b)
0.1
0
-0.1
-0.2
-0.3
-0.4
-0.5
-0.6
-0.7
1 2 3 4 5 6
(c)
1
0.8
0.6
0.4
0.2
0
-0.2
1 2 3 4 5 6
(d)
0.6
0.4
0.2
0
-0.2
-0.4
-0.6
-0.8
1 2 3 4 5 6

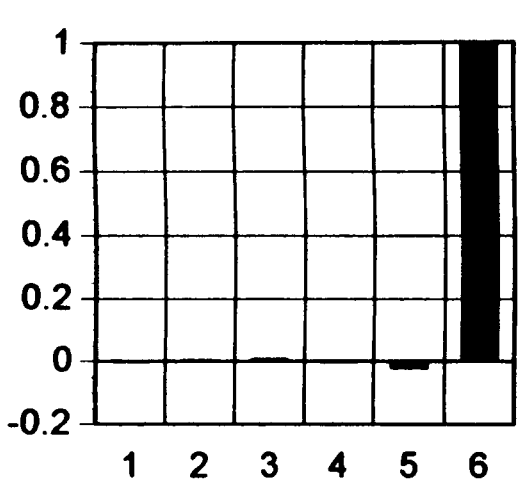
1
0.8
0.6
0.4
0.2
0
-0.2
1 2 3 4 5 6

(a)

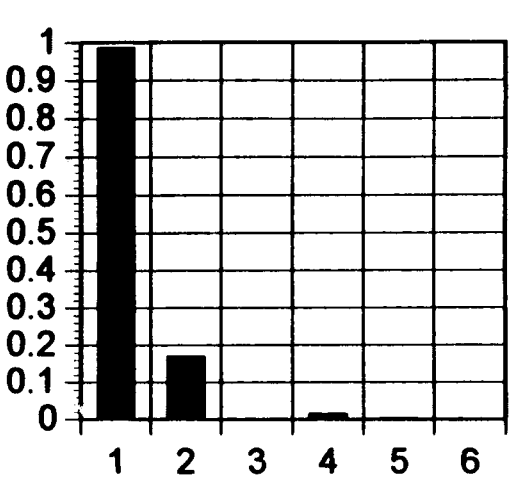
1
0.9
0.8
0.7
0.6
0.5
0.4
0.3
0.2
0.1
0
1 2 3 4 5 6

(b)

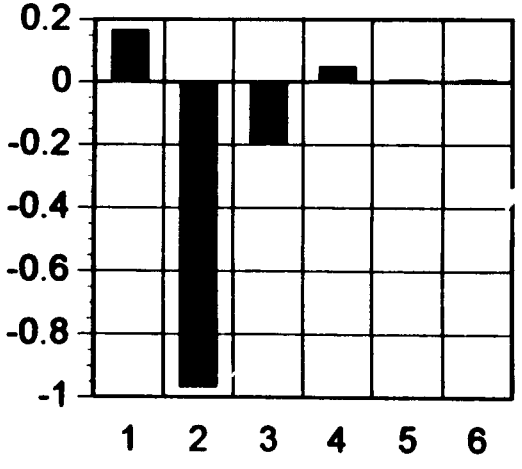
0.2
0
-0.2
-0.4
-0.6
-0.8
-1
1 2 3 4 5 6

(c)

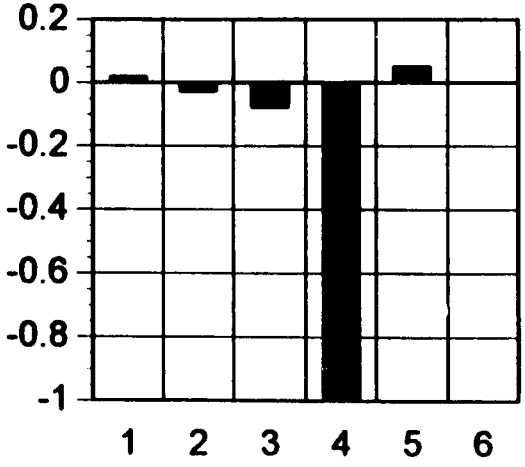
0.2
0
-0.2
-0.4
-0.6
-0.8
-1
1 2 3 4 5 6

(d)

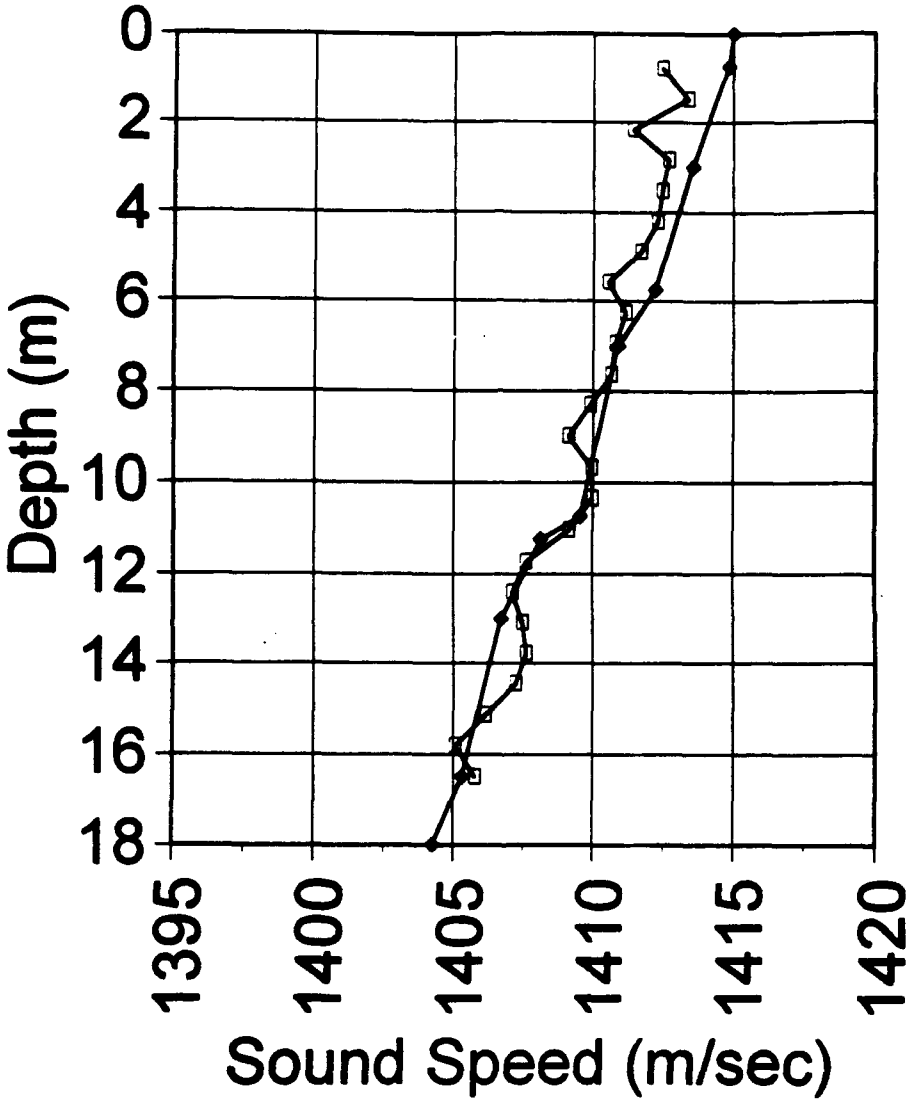
Depth (m)
0
2
4
6
8
10
12
14
16
18
1395
1400
1405
1410
1415
1420
Sound Speed (m/sec)

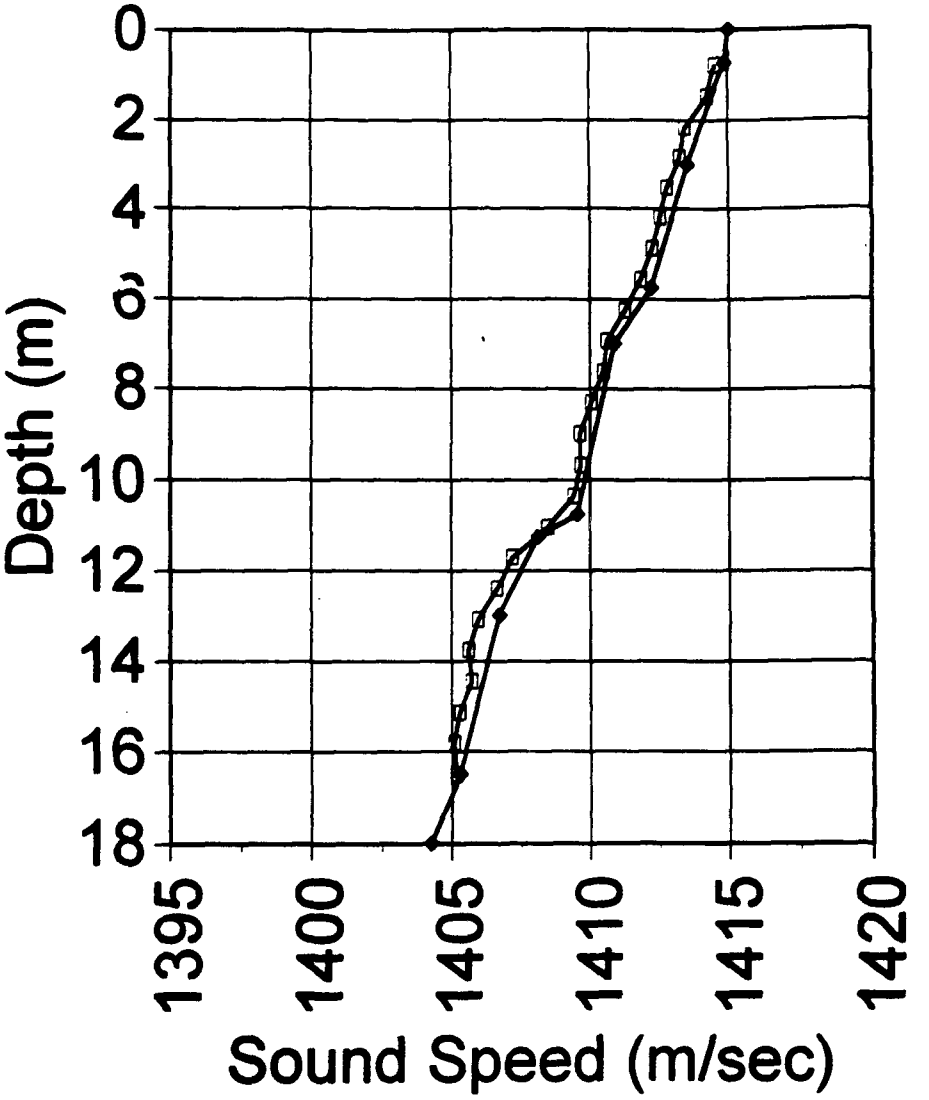
Depth (m)
0
2
4
6
8
10
12
14
16
18
1395
1400
1405
1410
1415
1420
Sound Speed (m/sec)

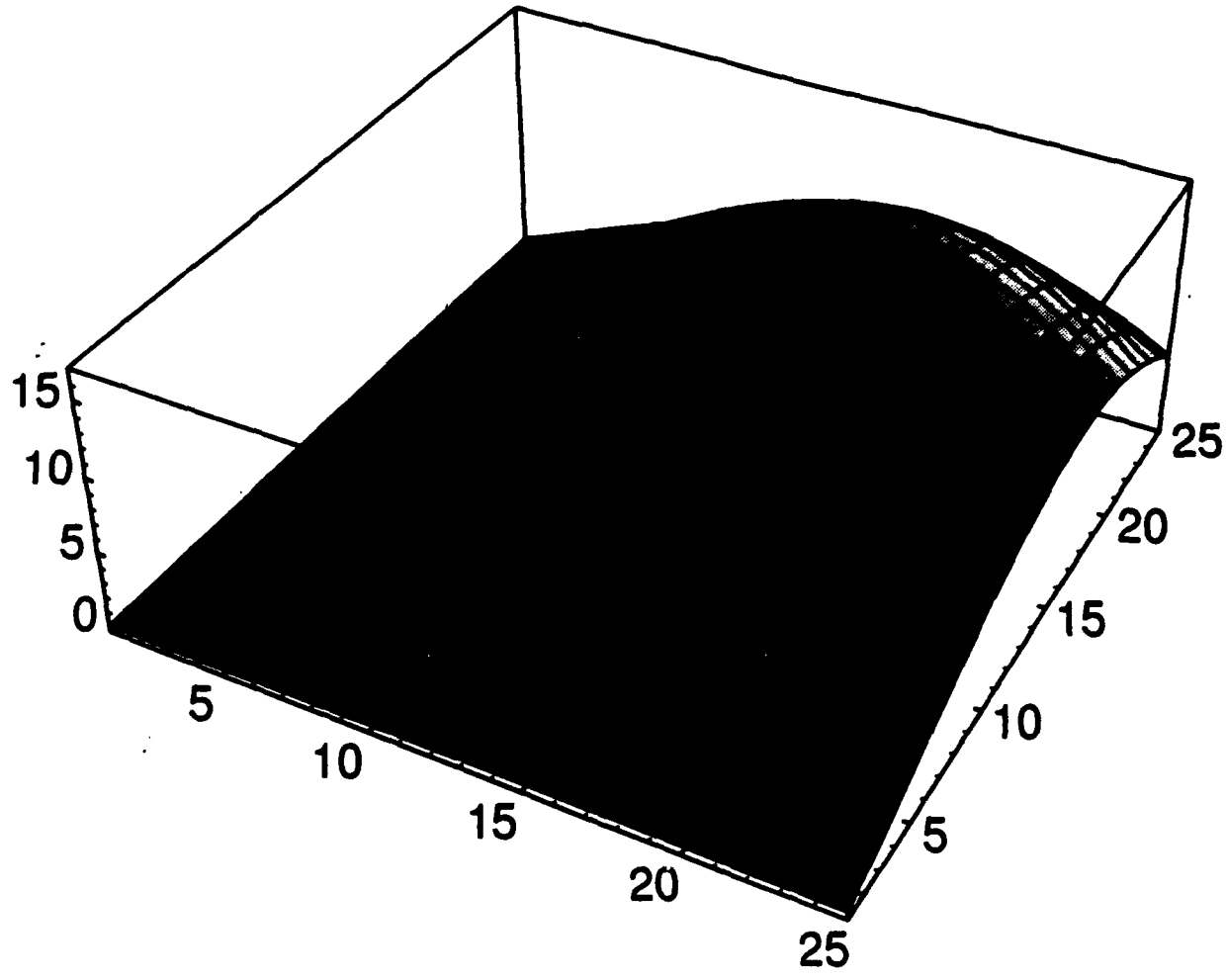

F. 6

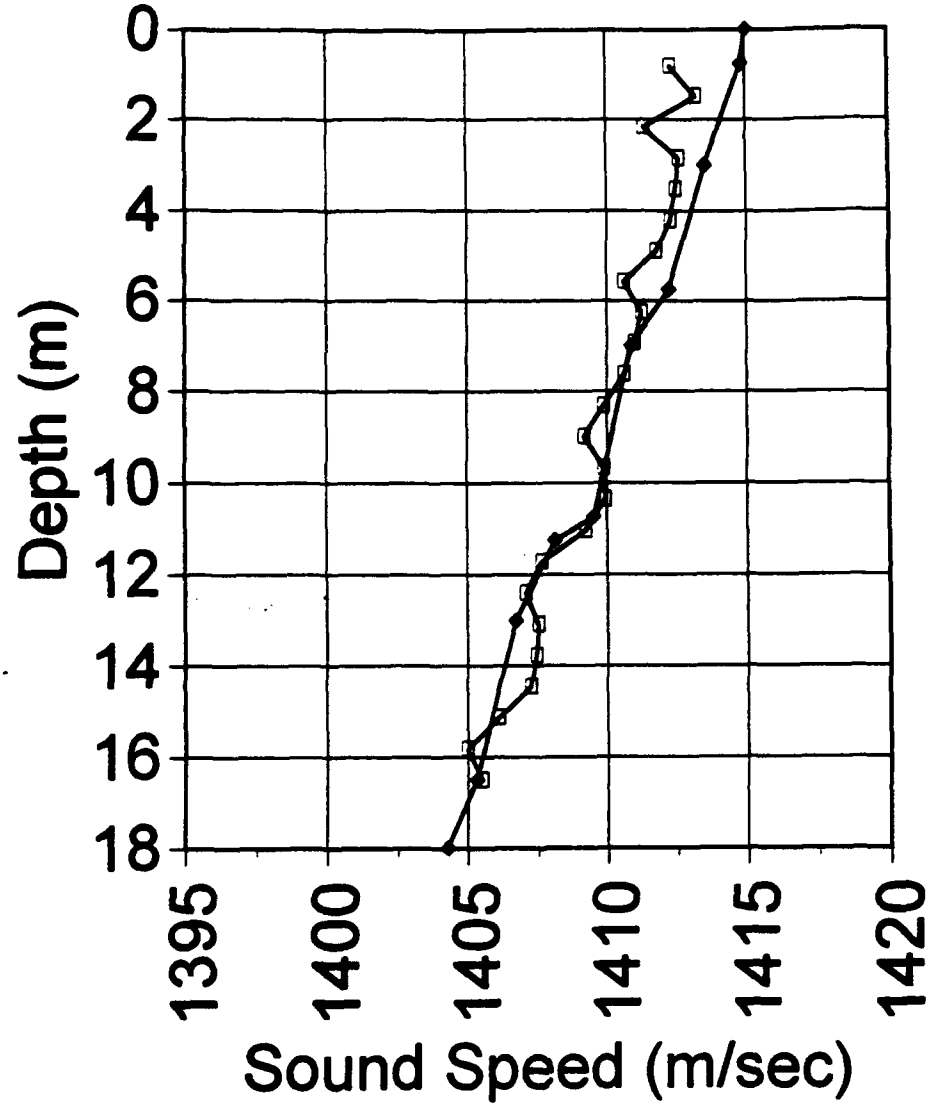
Depth (m)
0
2
4
6
8
10
12
14
16
18
1395
1400
1405
1410
1415
1420
Sound Speed (m/sec)

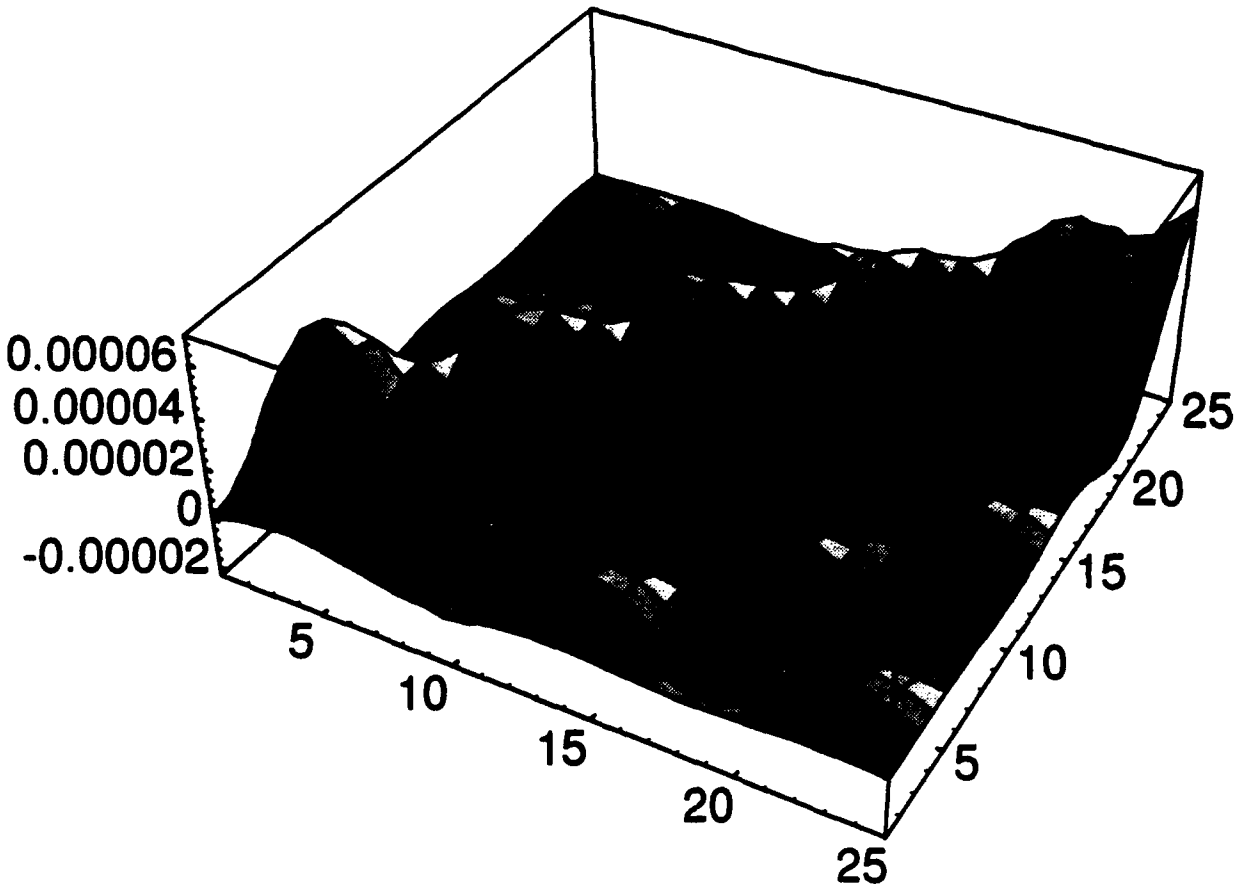

F 3 5

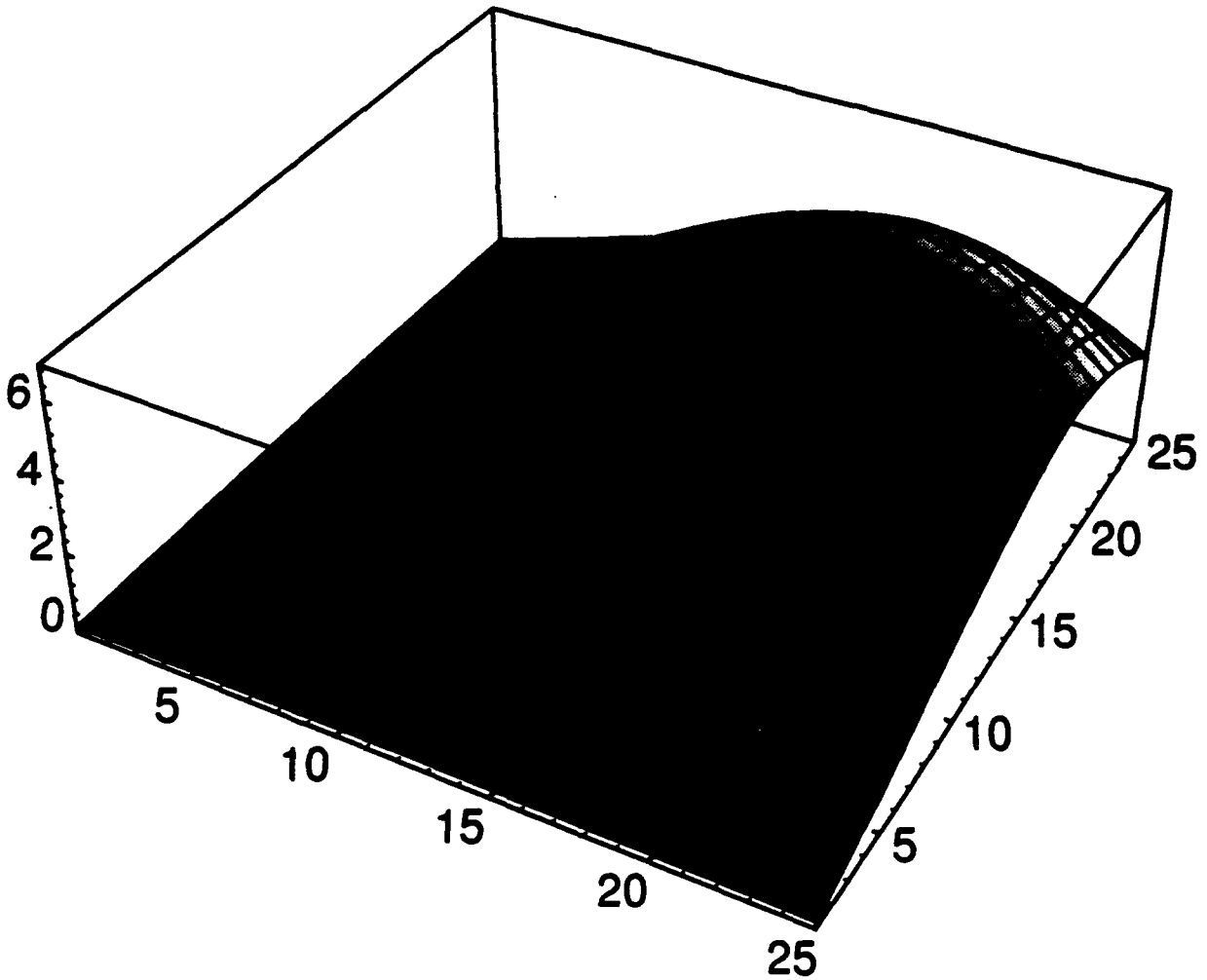
6
4
2
0
5
10
15
20
25
5
10
15
20
25

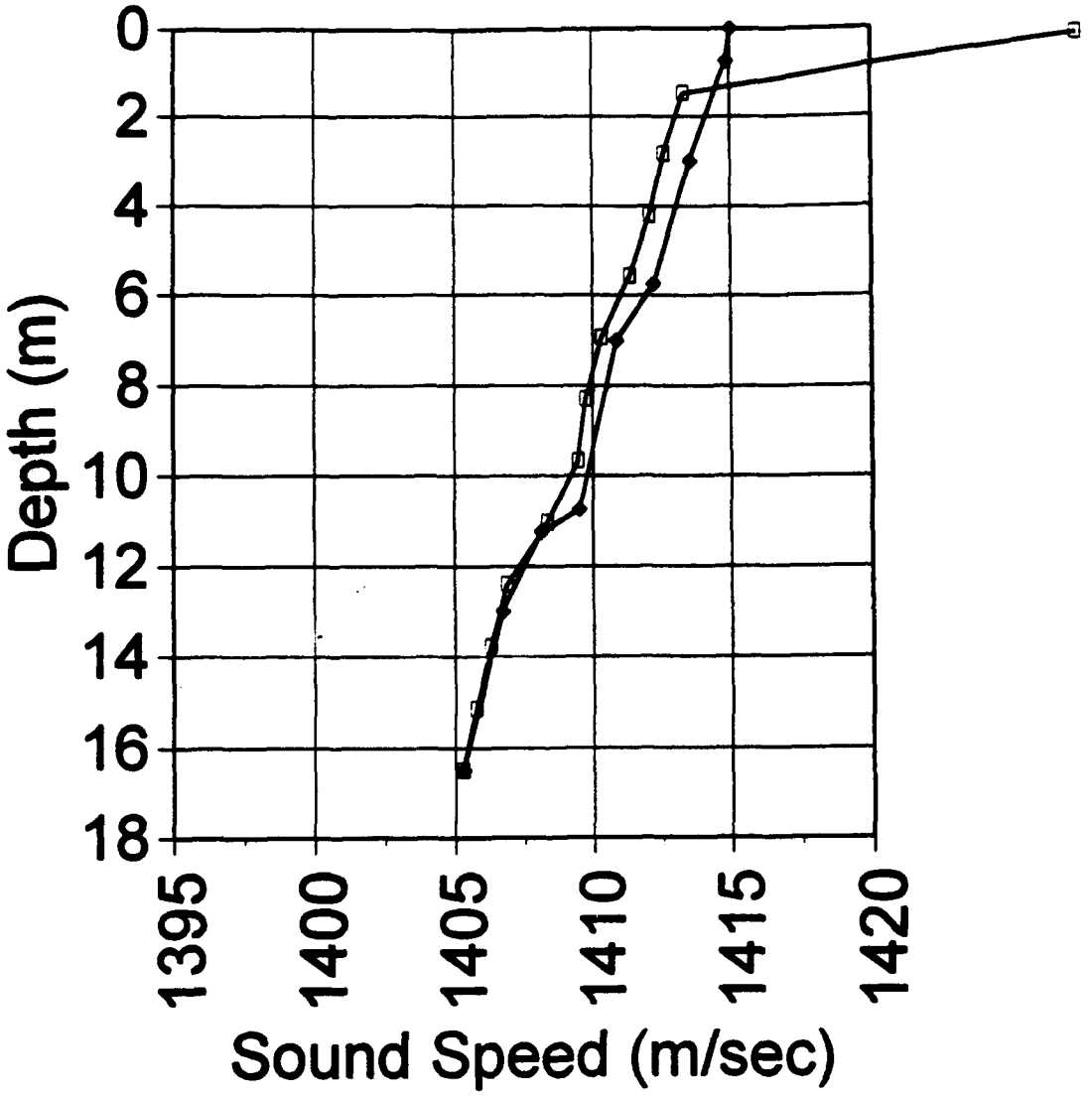
Depth (m)
0
2
4
6
8
10
12
14
16
18
1395
1400
1405
1410
1415
1420
Sound Speed (m/sec)

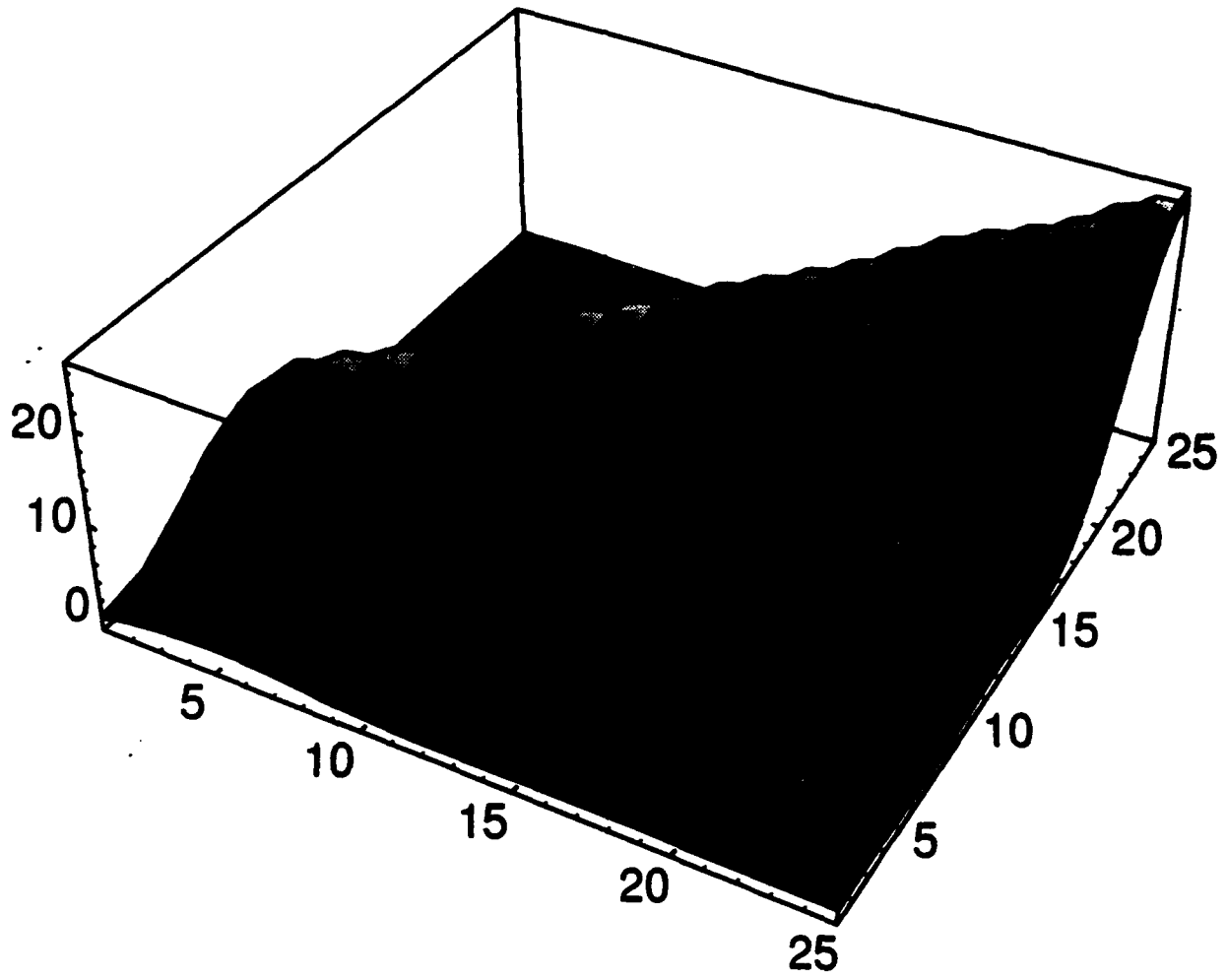
20
10
0
5
10
15
20
25
25
20
15
10
5

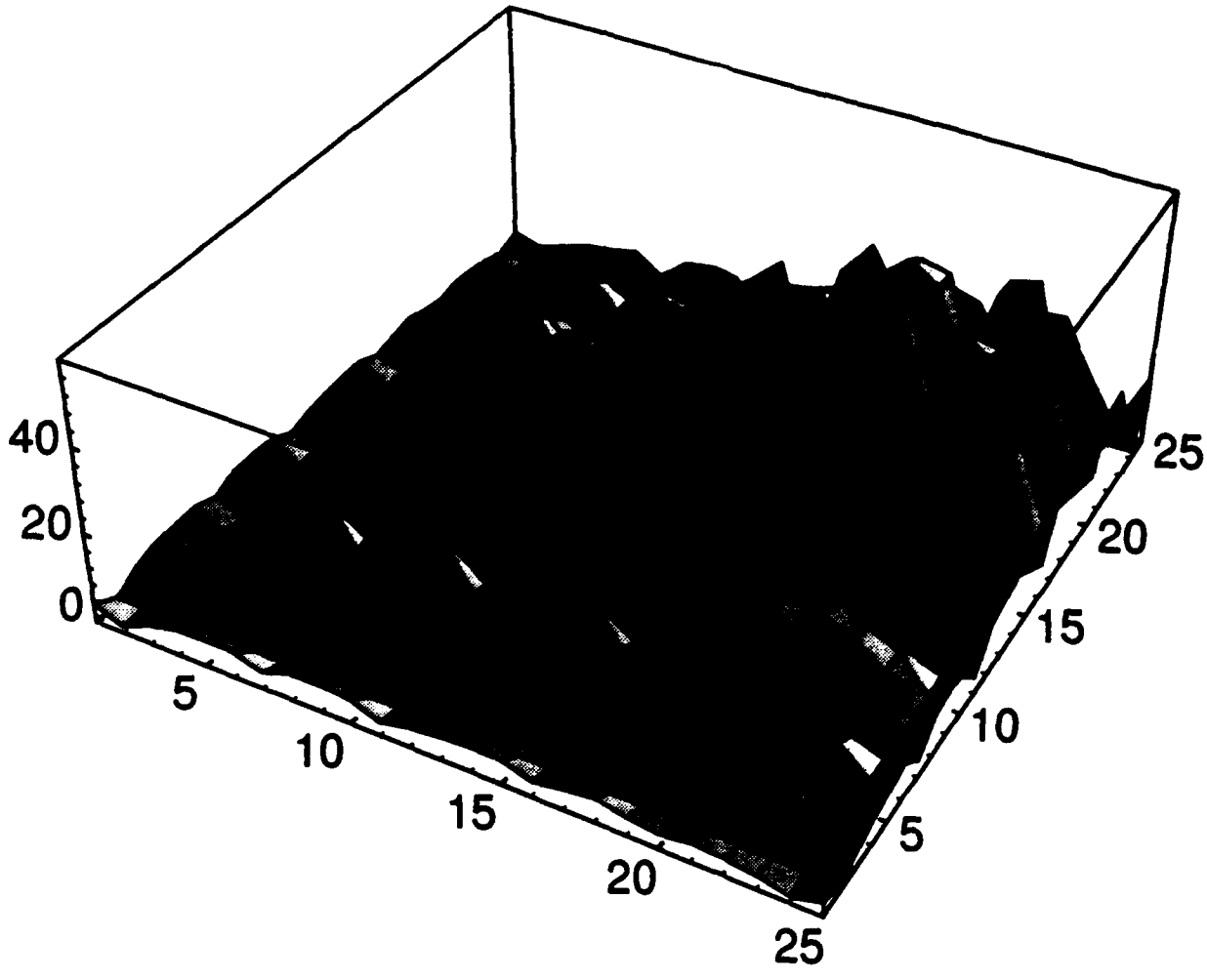
40
20
0
5
10
15
20
25
5
10
15
20
25

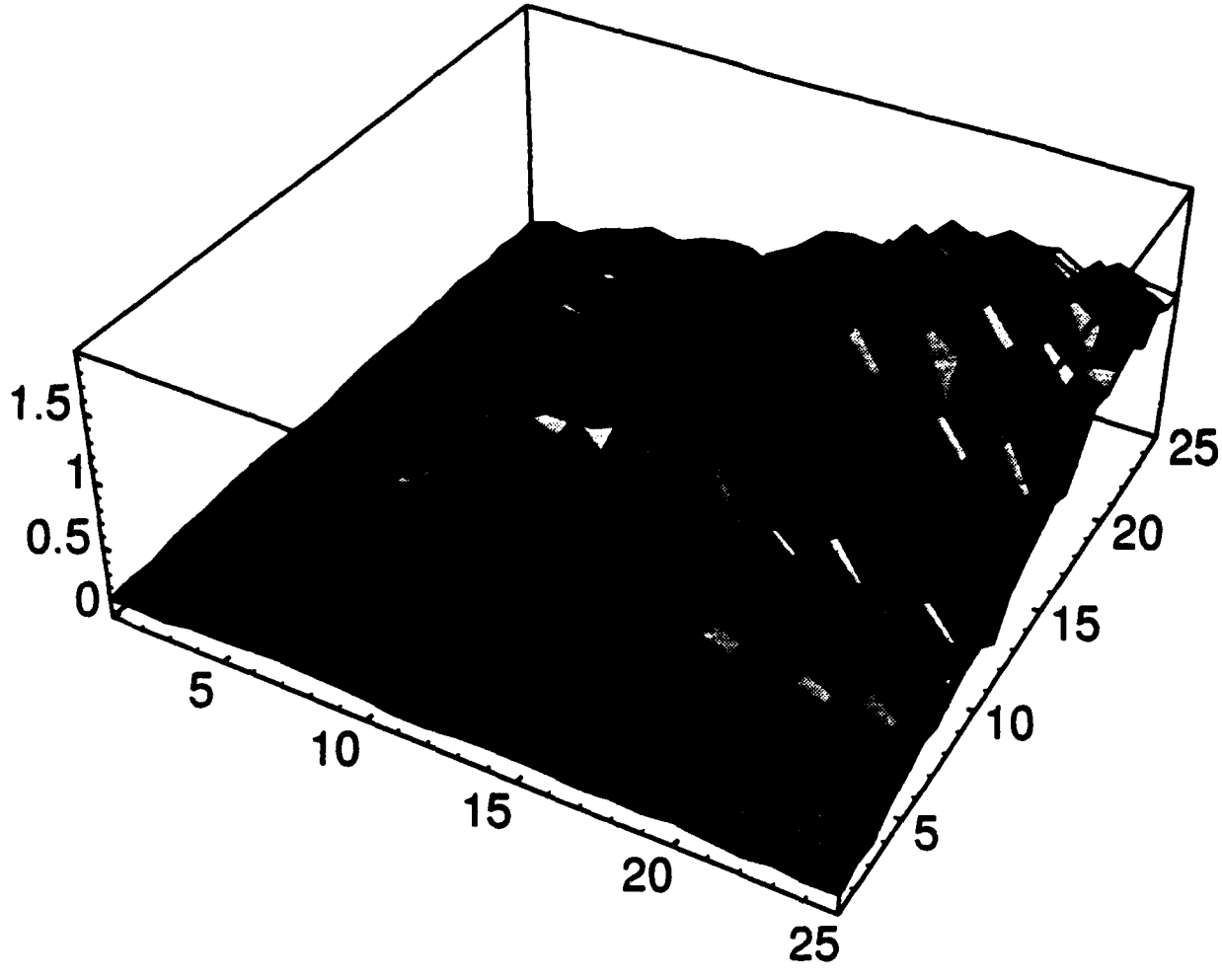
1.5
1
0.5
0
5
10
15
20
25
5
10
15
20
25

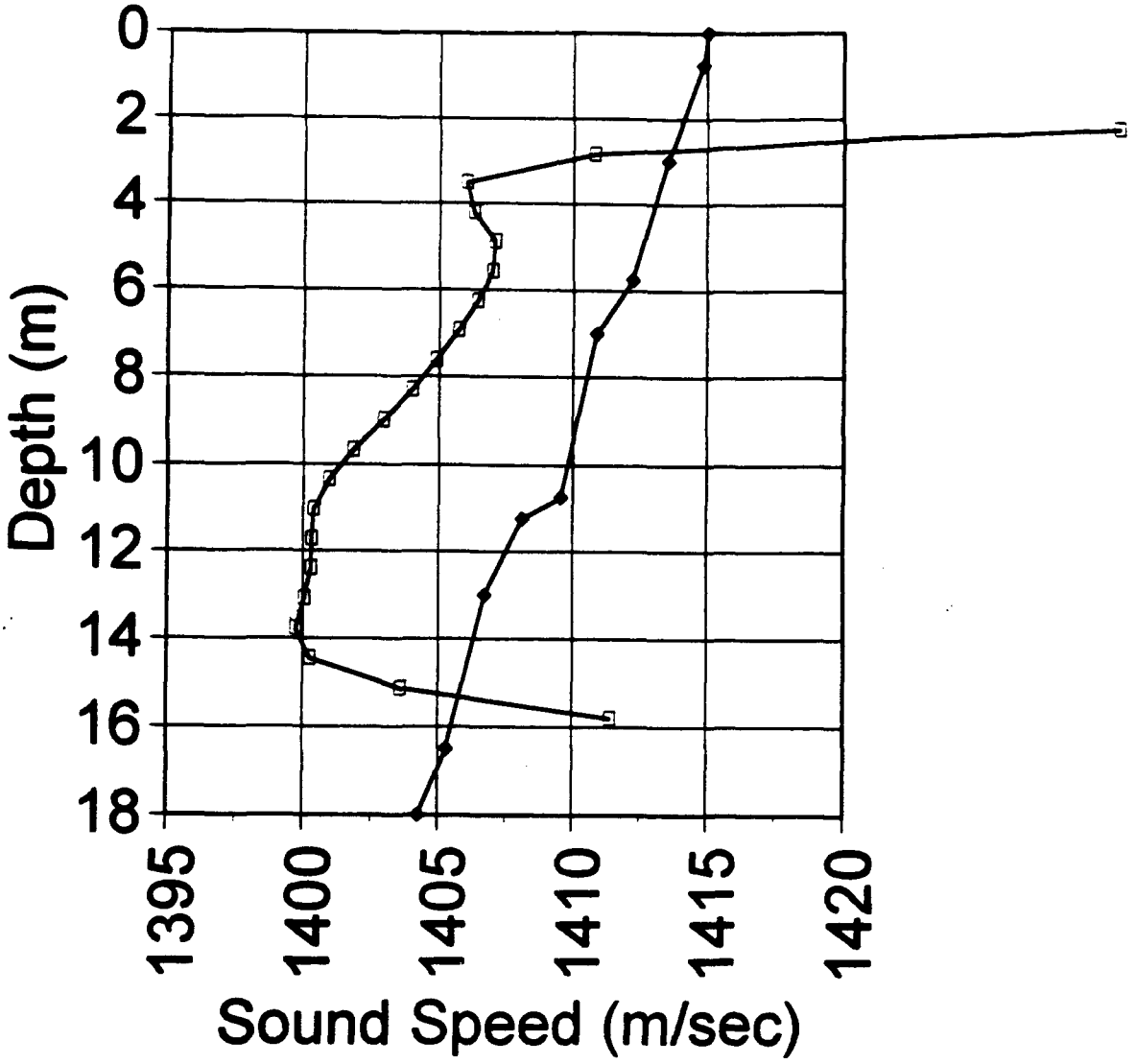
Depth (m)
0
2
4
6
8
10
12
14
16
18
1395
1400
1405
1410
1415
1420
Sound Speed (m/sec)

F.G. 2

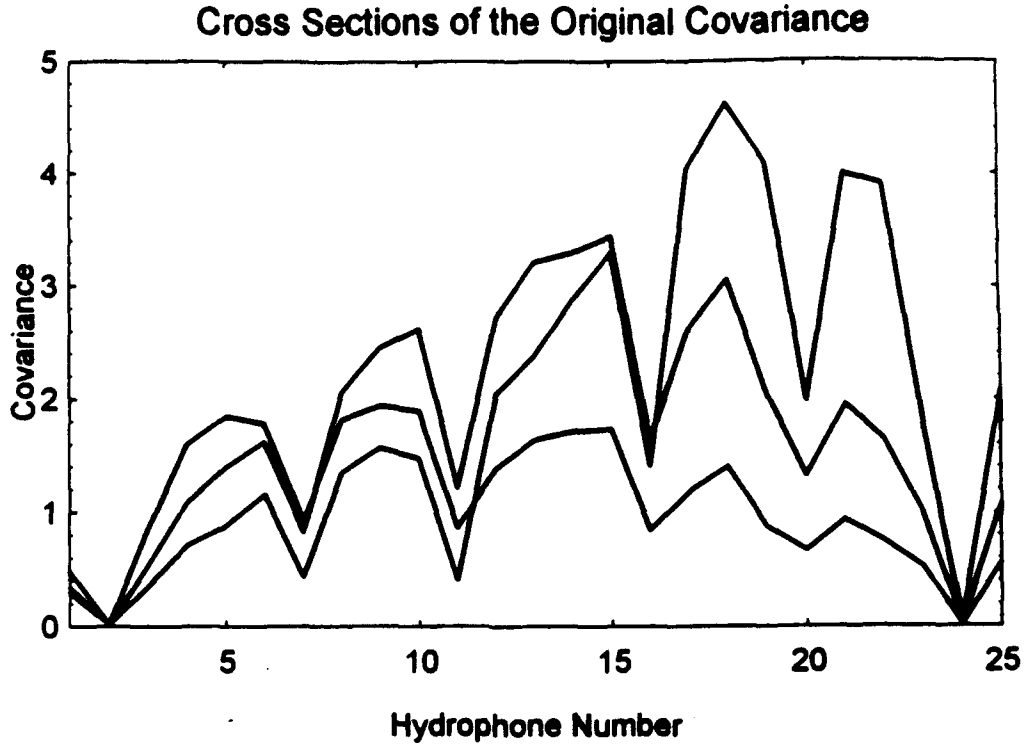
Cross Sections of the Original Covariance
Covariance
0
1
2
3
4
5
5
10
15
20
25
Hydrophone Number

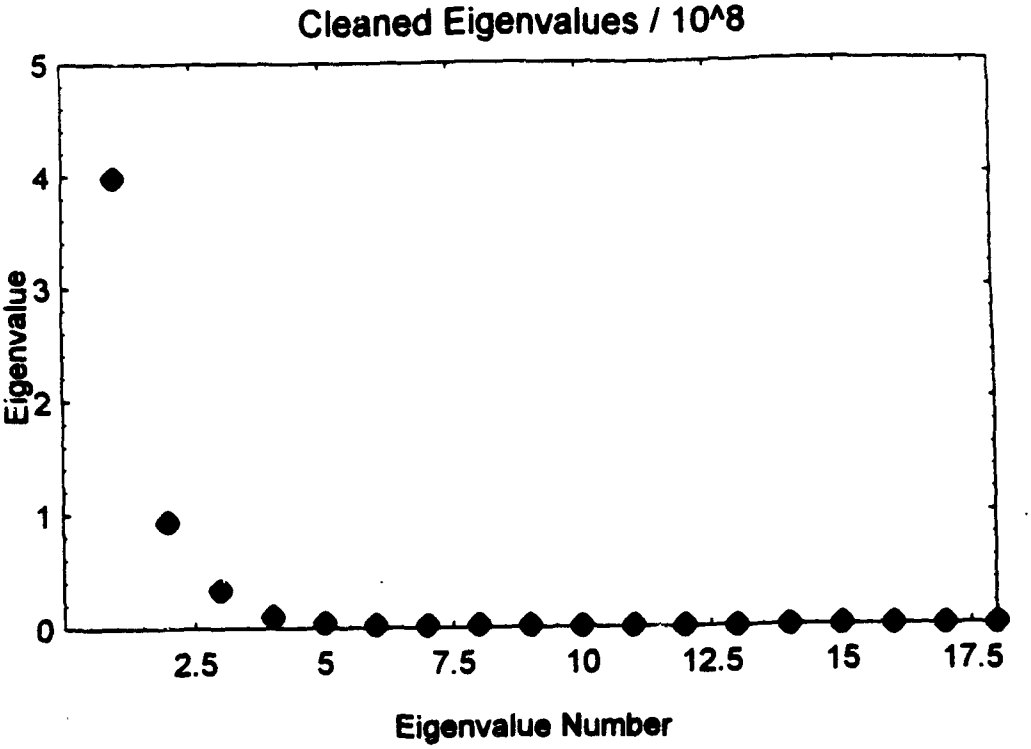
Cleaned Eigenvalues / 10^8
Eigenvalue
5
4
3
2
1
0
2.5
5
7.5
10
12.5
15
17.5
Eigenvalue Number

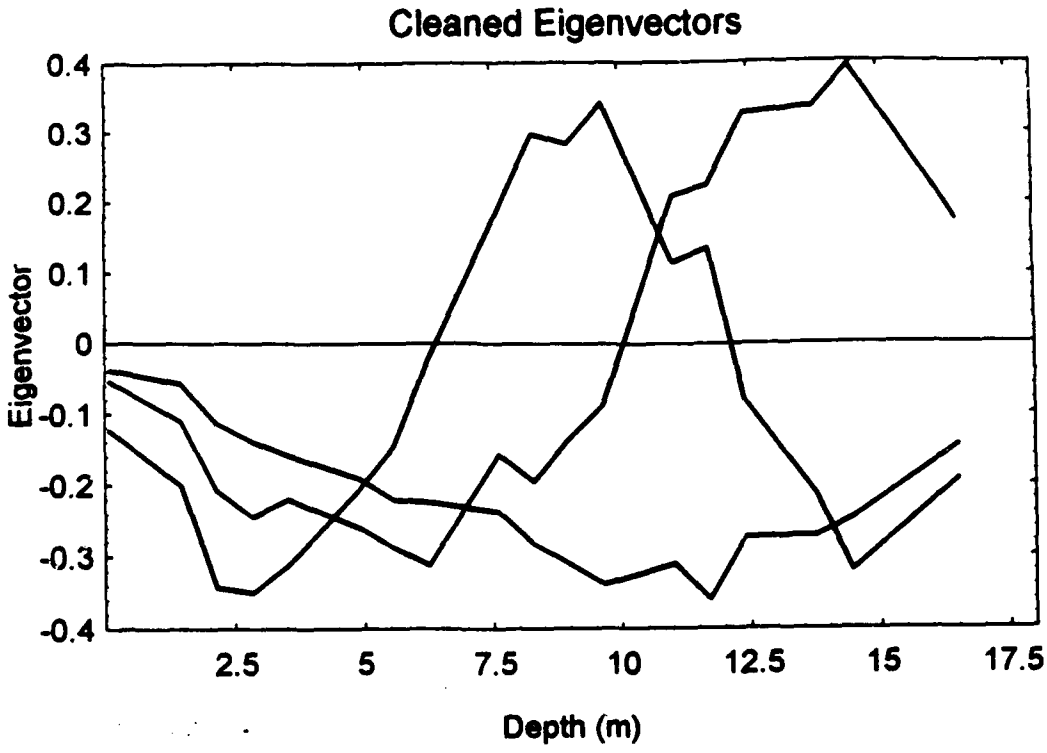
Cleaned Eigenvectors
0.4
0.3
0.2
0.1
0
-0.1
-0.2
-0.3
-0.4
Eigenvector
2.5
5
7.5
10
12.5
15
17.5
Depth (m)

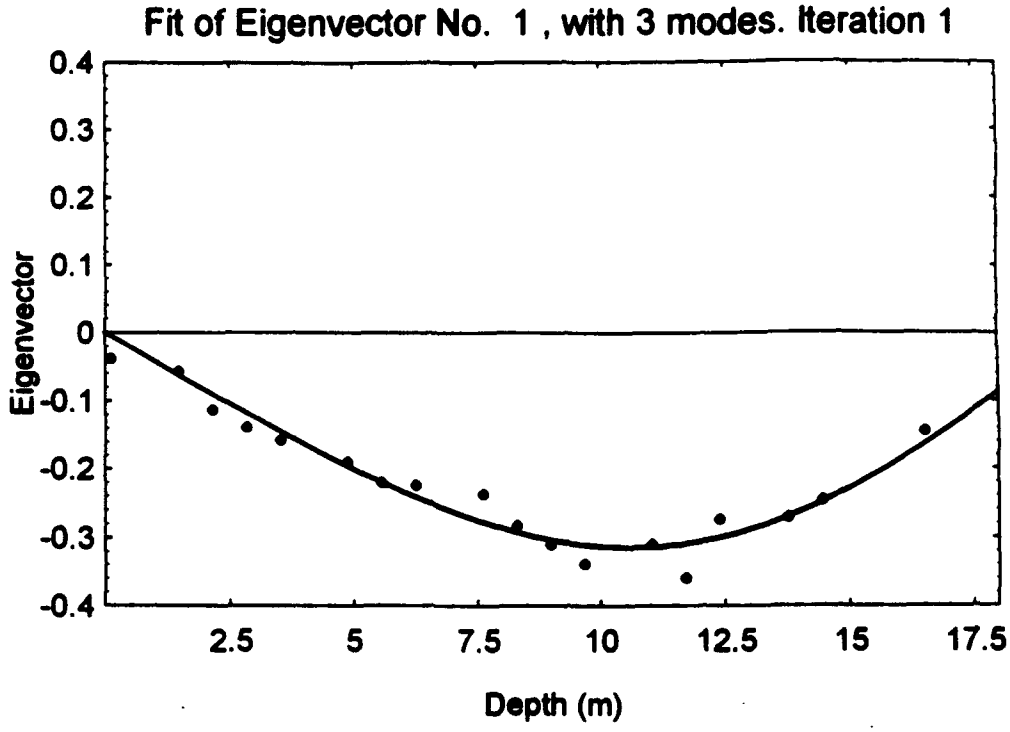
Fit of Eigenvector No. 1 , with 3 modes. Iteration 1
0.4
0.3
0.2
0.1
0
-0.1
-0.2
-0.3
-0.4
Eigenvector
2.5
5
7.5
10
12.5
15
17.5
Depth (m)

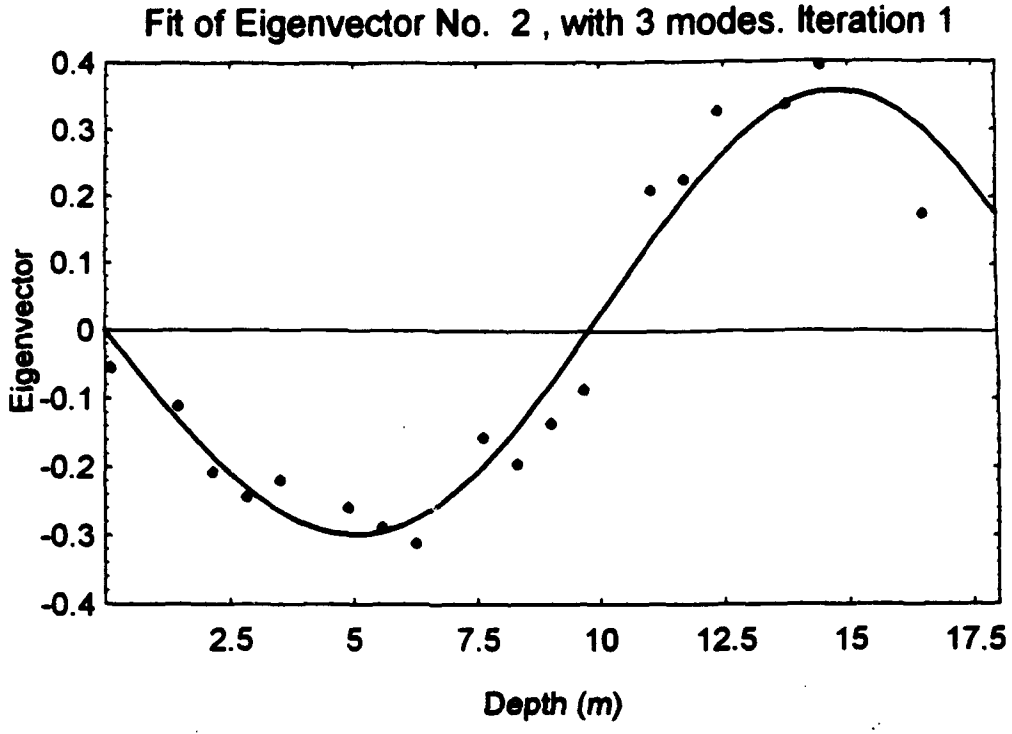
Fit of Eigenvector No. 2 , with 3 modes. Iteration 1
Eigenvector
0.4
0.3
0.2
0.1
0
-0.1
-0.2
-0.3
-0.4
2.5
5
7.5
10
12.5
15
17.5
Depth (m)

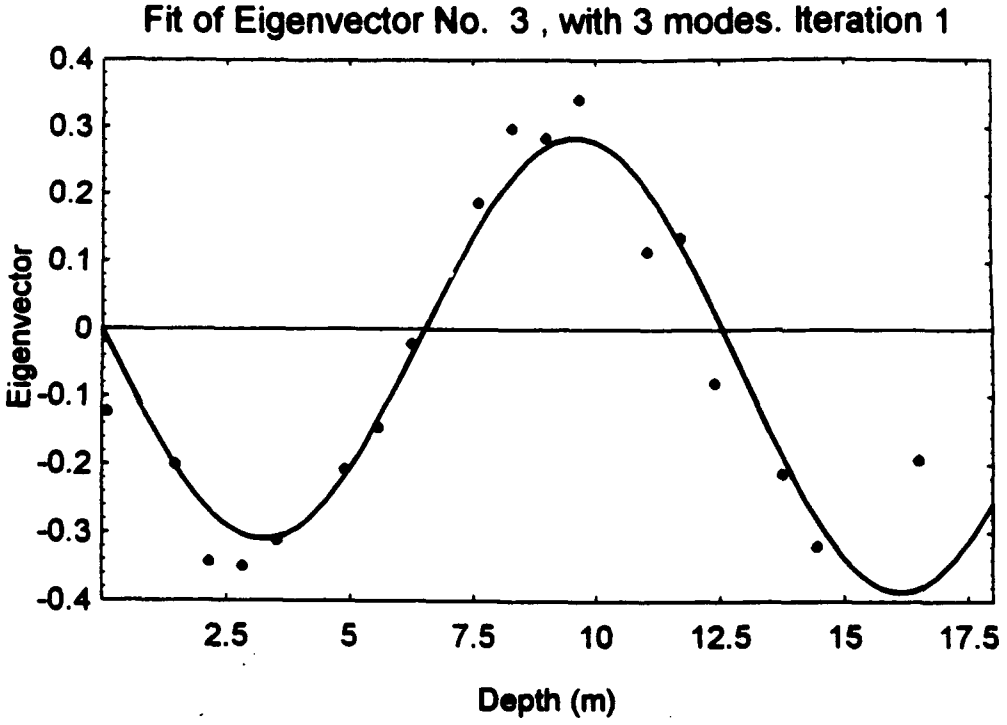
Fit of Eigenvector No. 3 , with 3 modes. Iteration 1
Eigenvector
0.4
0.3
0.2
0.1
0
-0.1
-0.2
-0.3
-0.4
2.5
5
7.5
10
12.5
15
17.5
Depth (m)

FIG 2C

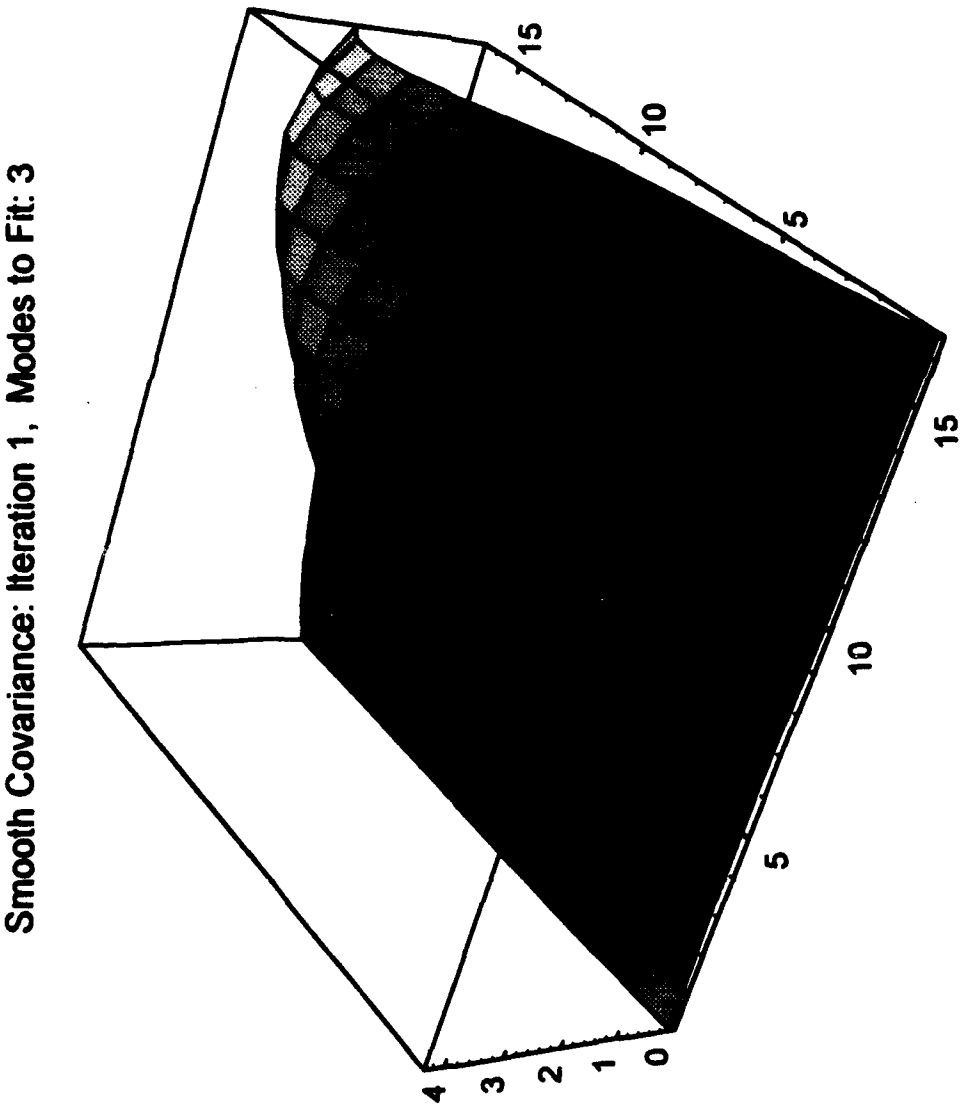
Smooth Covariance: Iteration 1, Modes to Fit: 3
15
10
5
15
10
5
4
3
2
1
0

FIG 12

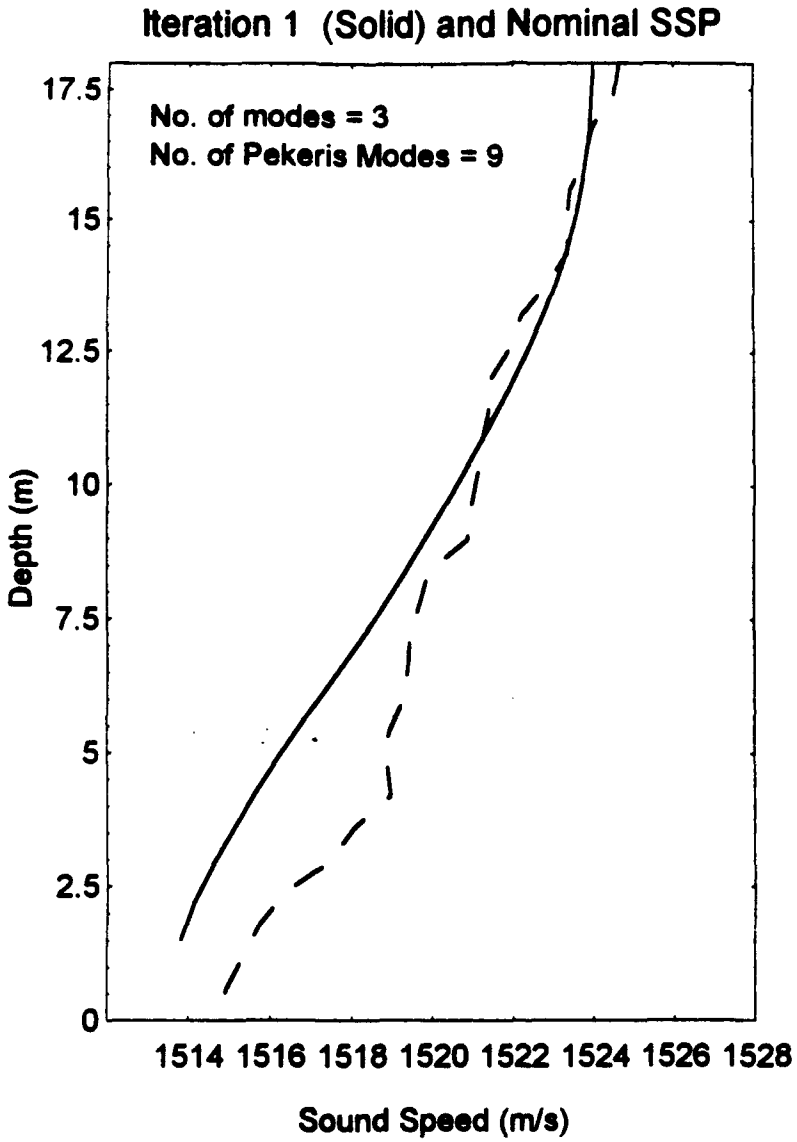
Iteration 1 (Solid) and Nominal SSP
No. of modes = 3
No. of Pekeris Modes = 9
17.5
15
12.5
10
7.5
5
2.5
0
Depth (m)
1514 1516 1518 1520 1522 1524 1526 1528
Sound Speed (m/s)

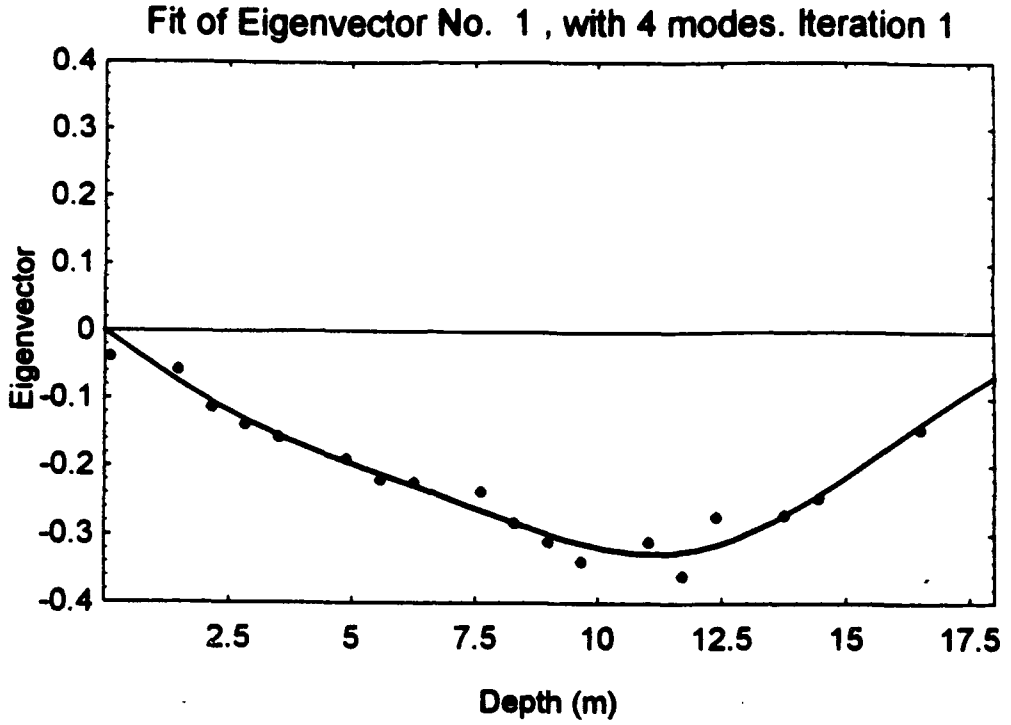
Fit of Eigenvector No. 1 , with 4 modes. Iteration 1
Eigenvector
0.4
0.3
0.2
0.1
0
-0.1
-0.2
-0.3
-0.4
2.5
5
7.5
10
12.5
15
17.5
Depth (m)

Fig 2.

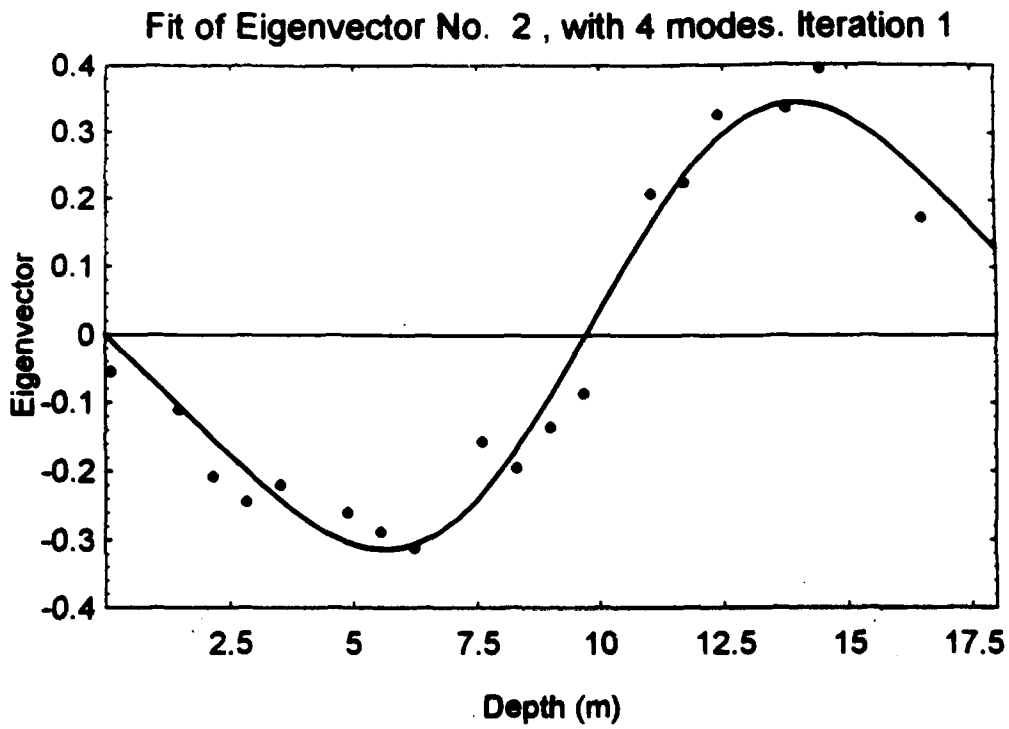
Fit of Eigenvector No. 2 , with 4 modes. Iteration 1
0.4
0.3
0.2
0.1
0
-0.1
-0.2
-0.3
-0.4
Eigenvector
2.5
5
7.5
10
12.5
15
17.5
Depth (m)

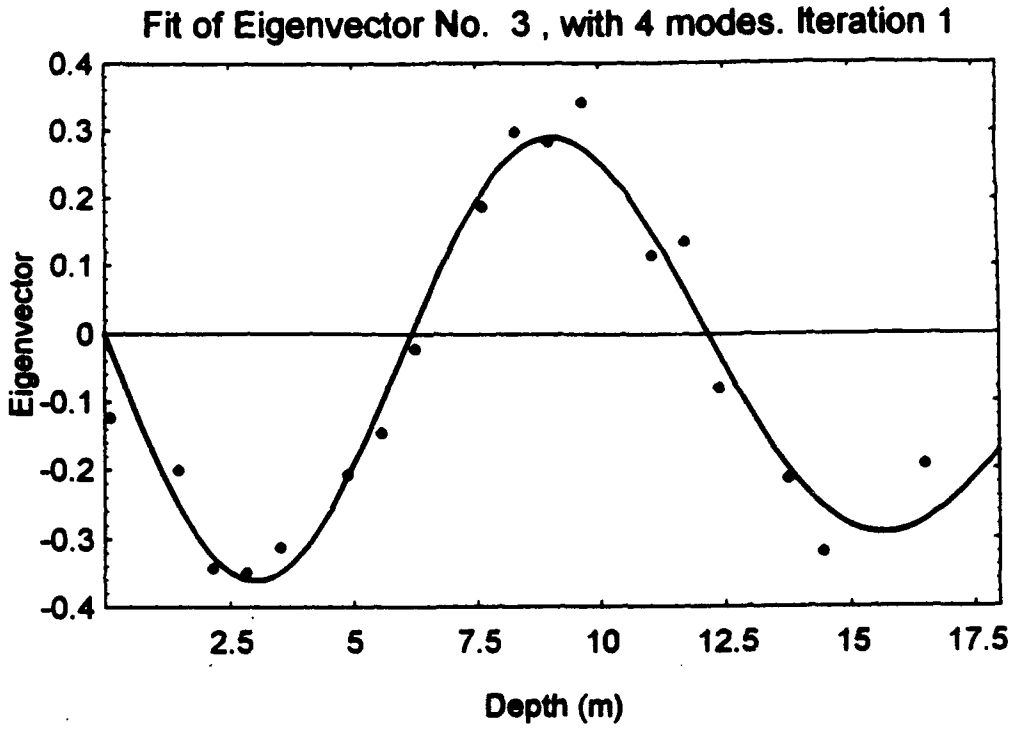
Fit of Eigenvector No. 3 , with 4 modes. Iteration 1
Eigenvector
0.4
0.3
0.2
0.1
0
-0.1
-0.2
-0.3
-0.4
2.5
5
7.5
10
12.5
15
17.5
Depth (m)

Fig 2C

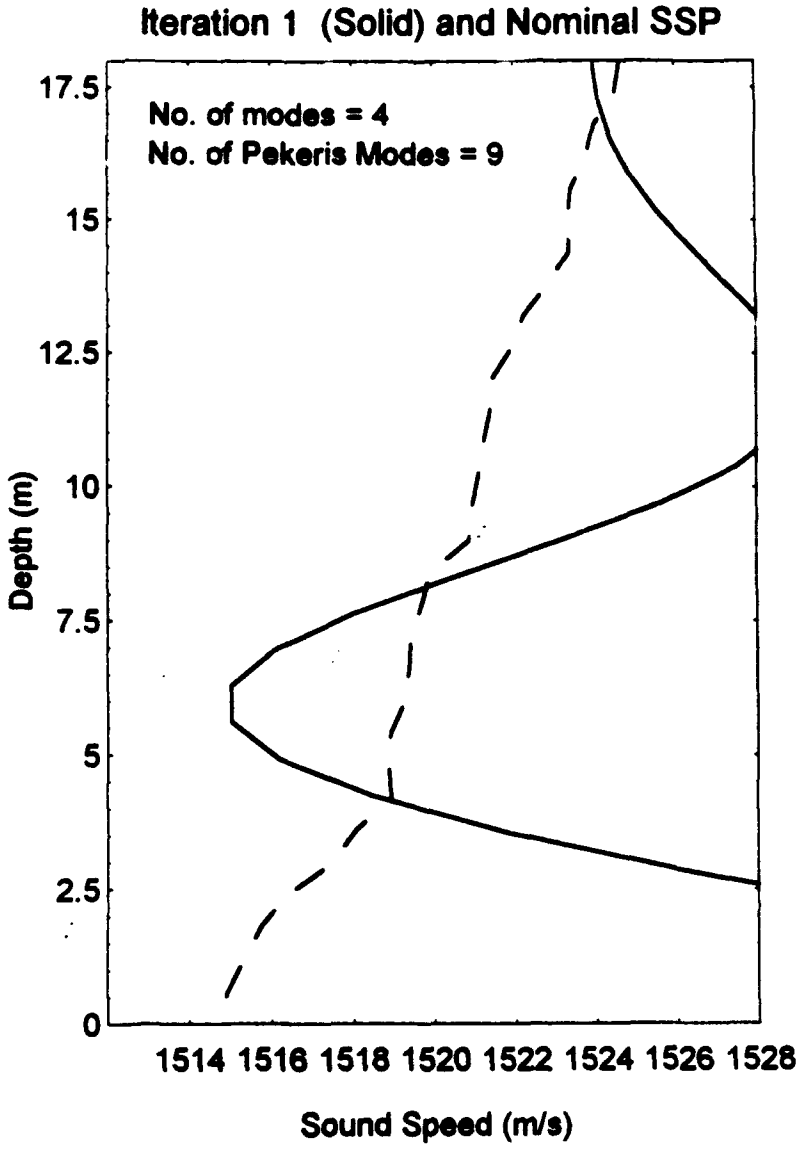
Iteration 1 (Solid) and Nominal SSP
No. of modes = 4
No. of Pekeris Modes = 9
17.5
15
12.5
10
7.5
5
2.5
0
Depth (m)
1514 1516 1518 1520 1522 1524 1526 1528
Sound Speed (m/s)

Fig 21

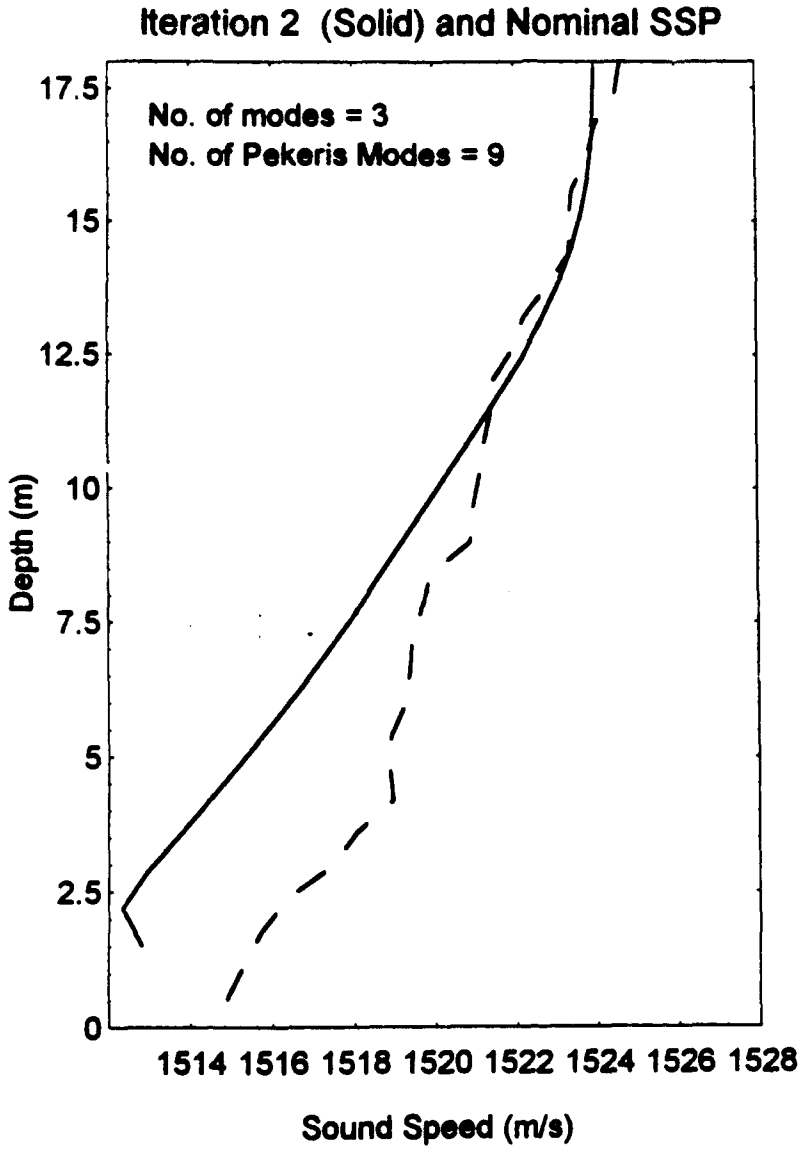
Iteration 2 (Solid) and Nominal SSP
No. of modes = 3
No. of Pekeris Modes = 9
17.5
15
12.5
10
7.5
5
2.5
0
Depth (m)
1514 1516 1518 1520 1522 1524 1526 1528
Sound Speed (m/s)

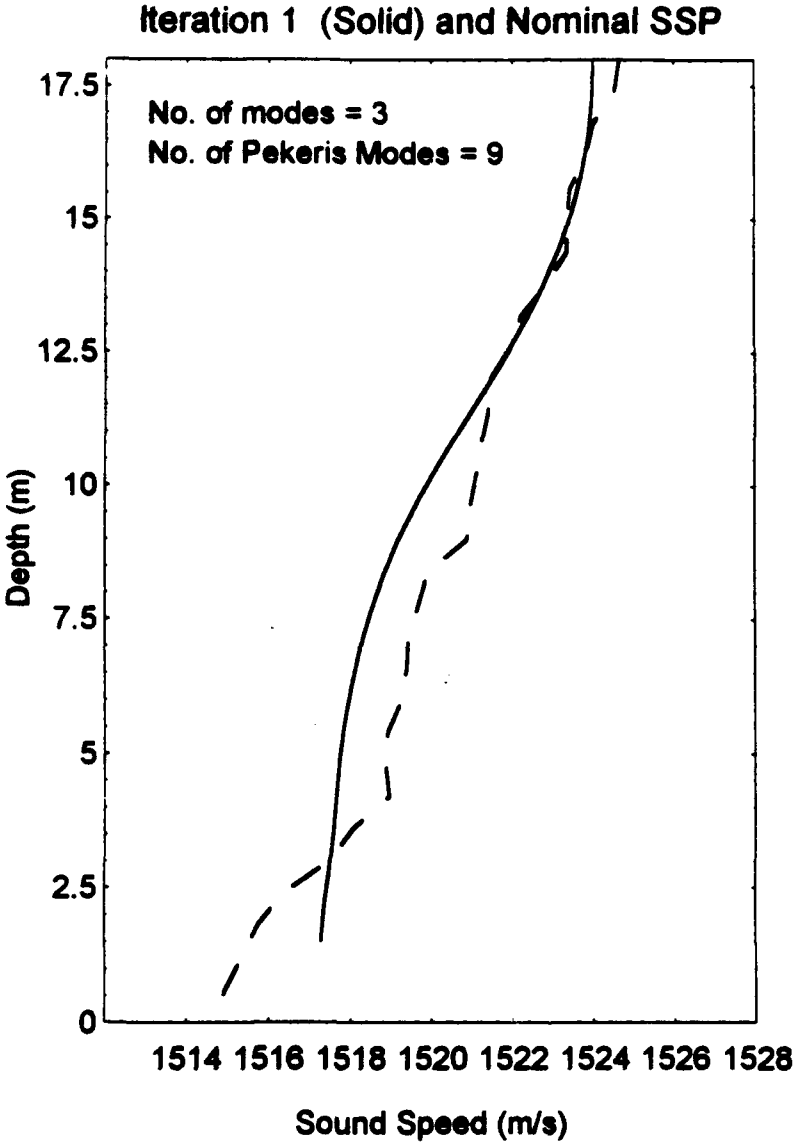
Iteration 1 (Solid) and Nominal SSP
No. of modes = 3
No. of Pekeris Modes = 9
17.5
15
12.5
10
7.5
5
2.5
0
Depth (m)
1514 1516 1518 1520 1522 1524 1526 1528
Sound Speed (m/s)

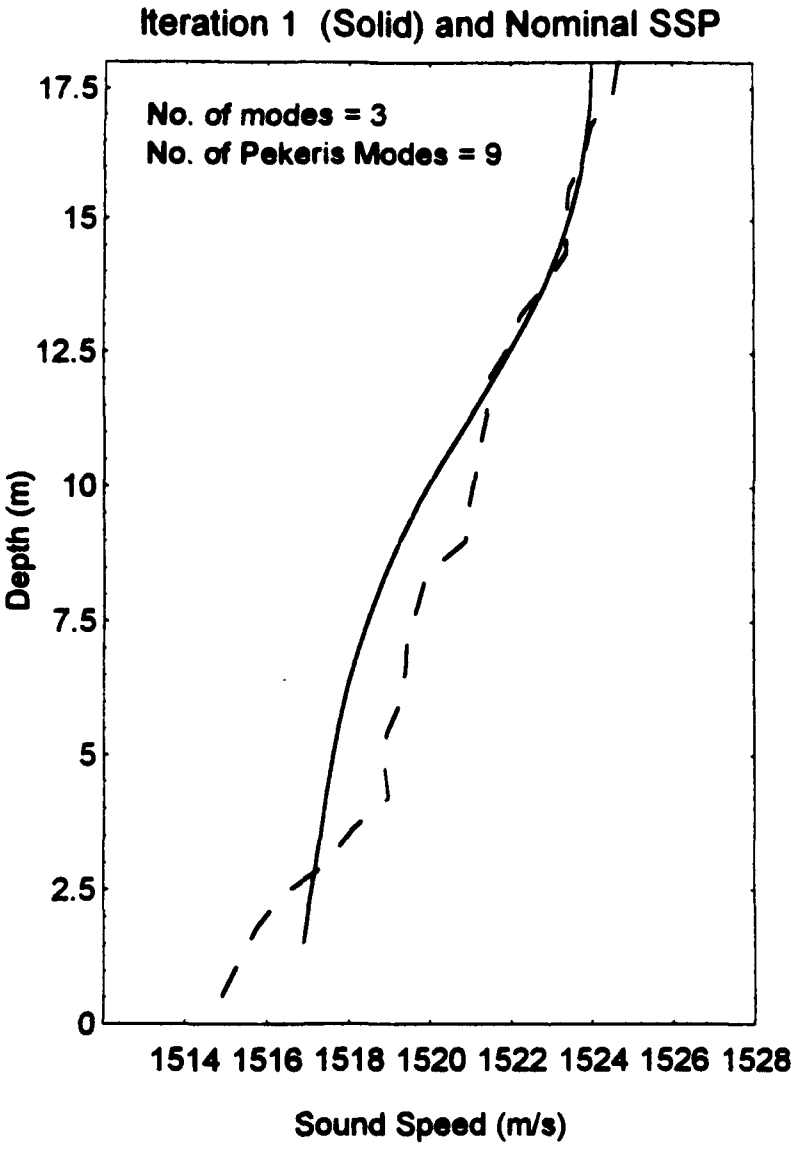
Iteration 1 (Solid) and Nominal SSP
No. of modes = 3
No. of Pekeris Modes = 9
17.5
15
12.5
10
7.5
5
2.5
0
Depth (m)
1514 1516 1518 1520 1522 1524 1526 1528
Sound Speed (m/s)

Fig 24

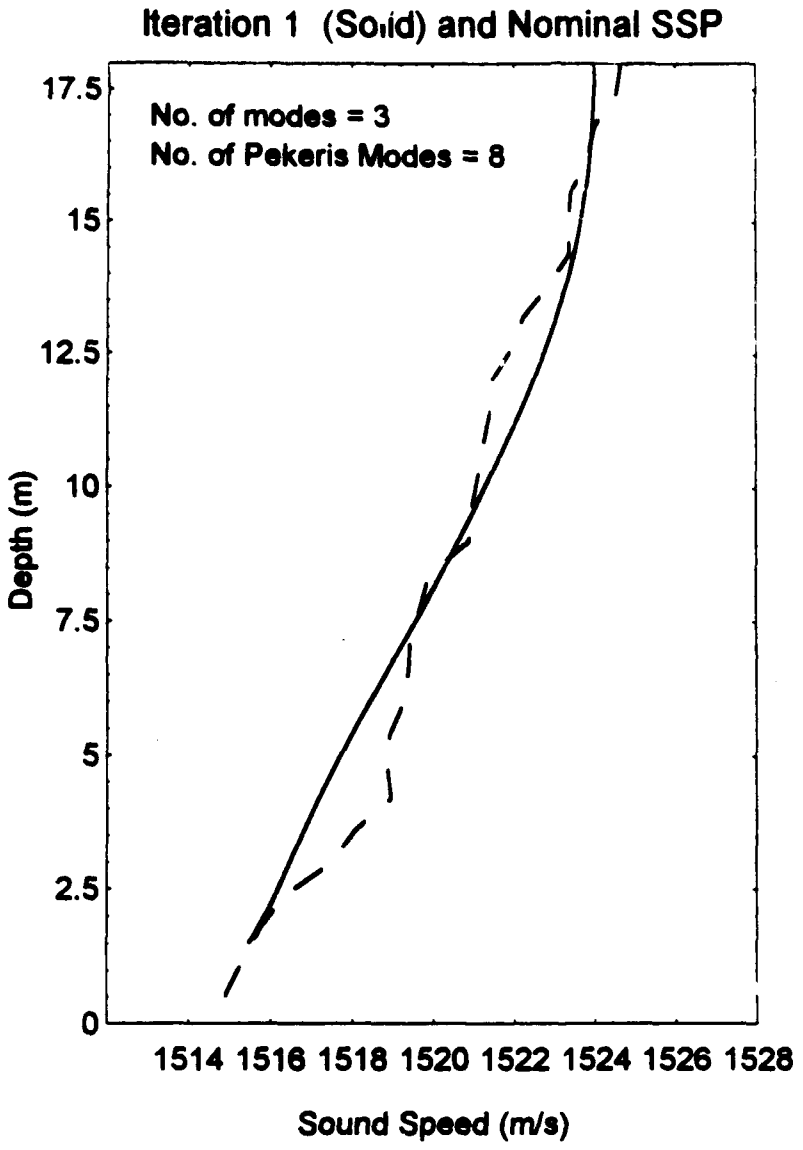
Iteration 1 (Solid) and Nominal SSP
No. of modes = 3
No. of Pekeris Modes = 8
17.5
15
12.5
10
7.5
5
2.5
0
Depth (m)
1514 1516 1518 1520 1522 1524 1526 1528
Sound Speed (m/s)

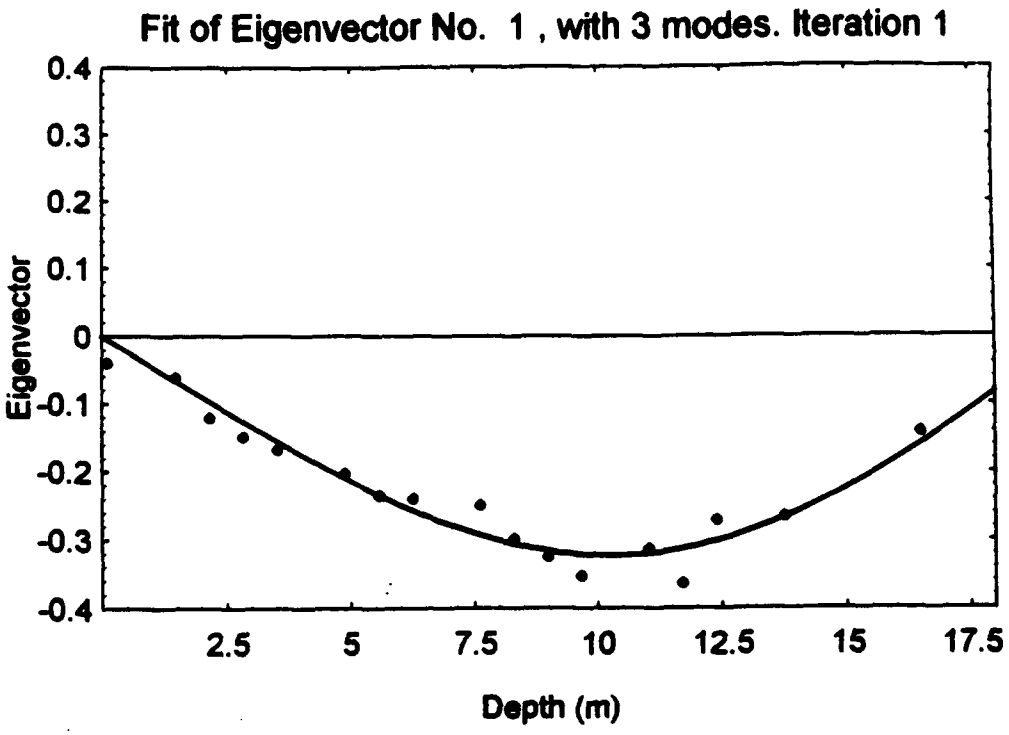
Fit of Eigenvector No. 1 , with 3 modes. Iteration 1
0.4
0.3
0.2
0.1
0
-0.1
-0.2
-0.3
-0.4
Eigenvector
2.5
5
7.5
10
12.5
15
17.5
Depth (m)

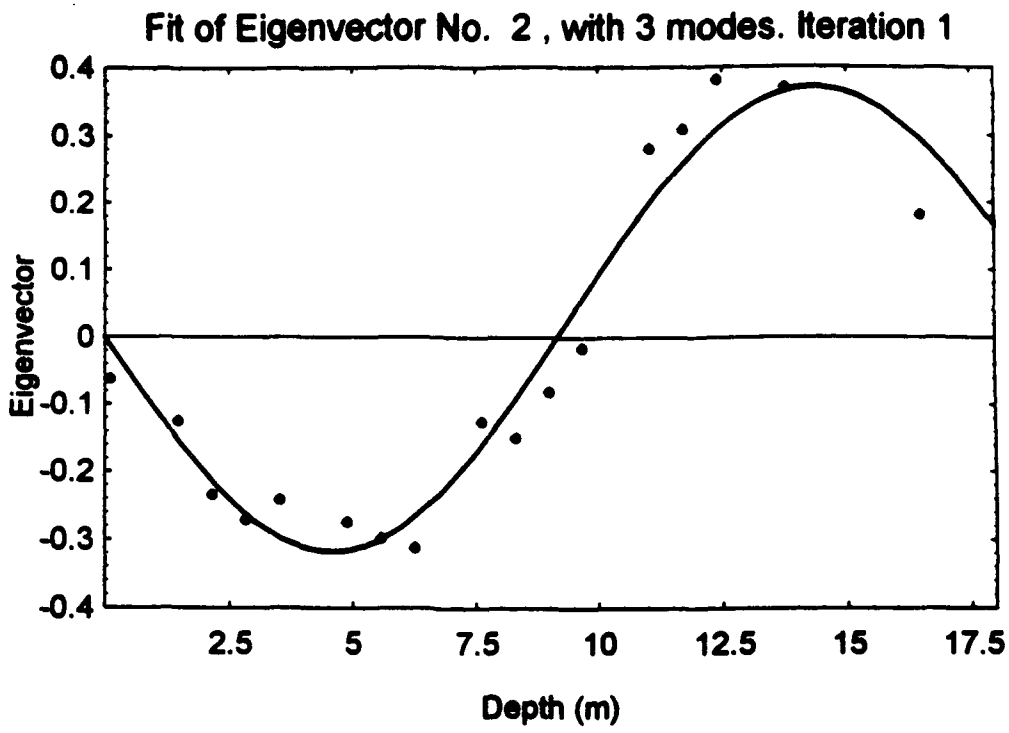
Fit of Eigenvector No. 2 , with 3 modes. Iteration 1
Eigenvector
0.4
0.3
0.2
0.1
0
-0.1
-0.2
-0.3
-0.4
2.5
5
7.5
10
12.5
15
17.5
Depth (m)

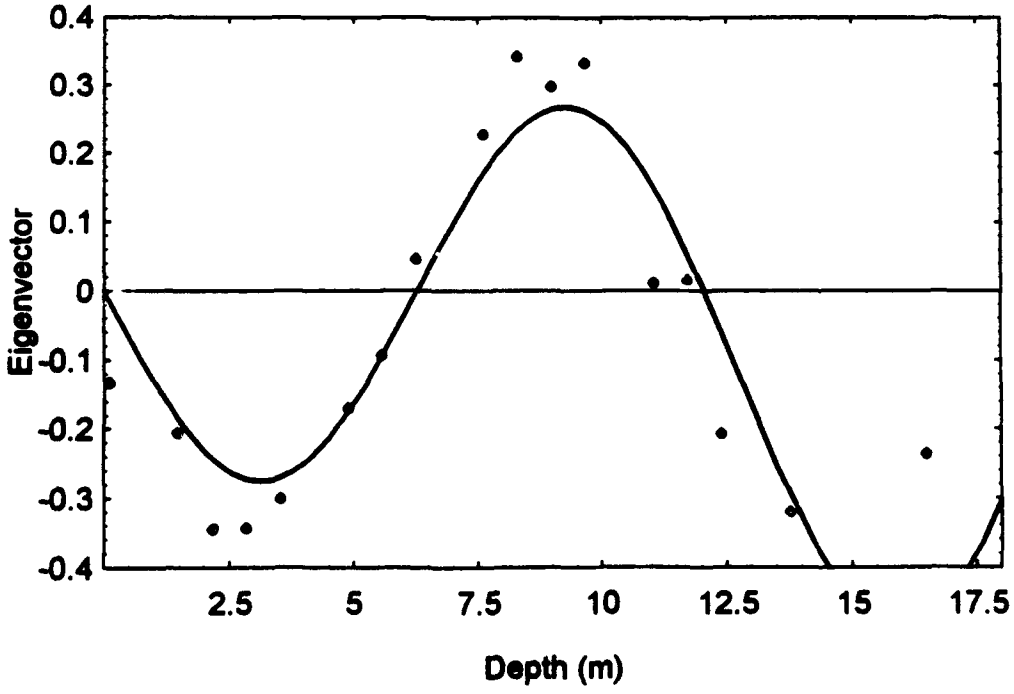
Fit of Eigenvector No. 3 , with 3 modes. Iteration 1
Eigenvector
0.4
0.3
0.2
0.1
0
-0.1
-0.2
-0.3
-0.4
2.5
5
7.5
10
12.5
15
17.5
Depth (m)

FIG 2C , b, C

■ Without phones 22,23,24 using Hardramp.env

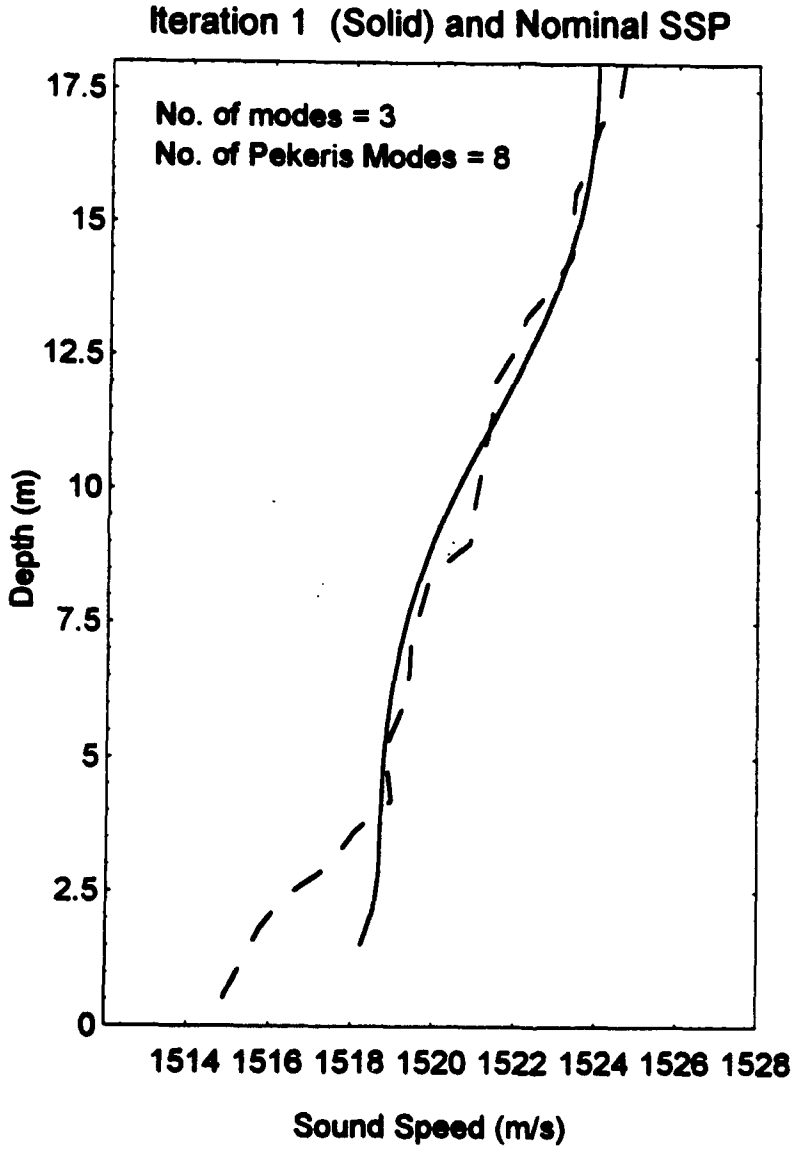

FIG 27

Without 22,23,24 starting from Hardramp.env

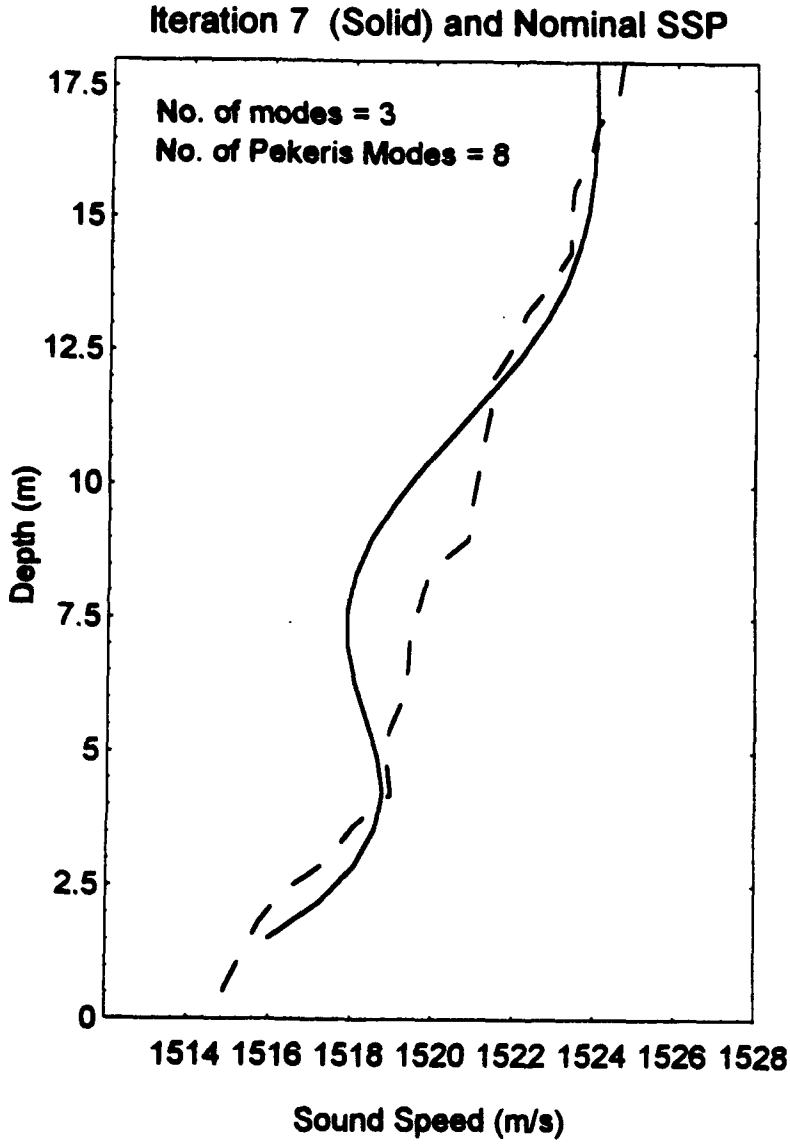

FIG 28